THESIS FOR THE DEGREE OF DOCTOR OF PHILOSOPHY

Thermal transport in van der Waals Solids and Inorganic Clathrates from first-principles calculations

DANIEL O. LINDROTH

Department of Physics
CHALMERS UNIVERSITY OF TECHNOLOGY
Göteborg, Sweden 2018

Thermal transport in
van der Waals Solids and Inorganic Clathrates
from first-principles calculations

Daniel O. Lindroth

isbn 978-91-7597-749-2

Doktorsavhandlingar vid Chalmers Tekniska Högskola
Ny serie nr 4430
ISSN 0346-718X

Department of Physics
Chalmers University of Technology
se-412 96 Göteborg, Sweden
Telephone +46 31 772 10 00

Typeset in XƎLaTeX with Times Ten and Akzidenz-Grotesk

Cover: The left jar displays a transition metal dichacogenide, disturbed by vibrations. In front are calculated results for the lattice thermal conductivity in WSe_2 and WS_2. The right jar displays the crystal structure of a type I clathrate. In front are the computed lifetimes for the clathrate $Ba_8Ga_{16}Ge_{30}$.

Chalmers reproservice
Göteborg, Sweden 2018

Thermal transport in van der Waals Solids and Inorganic Clathrates from first-principles calculations

DANIEL O. LINDROTH
Department of Physics
Chalmers University of Technology

Abstract

Energy management is arguably one of the defining challenges for our modern societies. An ever-increasing demand for energy has to be balanced with the requirement for a sustainable energy economy that minimizes the human impact on the environment. Materials and their ability to transport both electrical and thermal currents play a key role in this area as they are essential components in energy extraction, transport, storage, and consumption technologies. On the macroscopic level, electrical and thermal transport in materials can be described by a set of coupled phenomenological relations that contain material specific transport coefficients. On the microscopic level, these transport coefficients are governed by chemical composition and the specific arrangement of the constituent atoms, the so-called microstructure. Since relatively small differences in this regard can have a dramatic impact on the macroscopic behavior of a material, a detailed understanding of the underlying processes and couplings is essential for materials development and optimization.

In this thesis, the thermal conductivity in two classes of materials of current and future technological importance has been investigated using electronic structure calculations (density functional theory) in combination with methods from statistical physics (Boltzmann transport theory). The first two papers included in this thesis deal with van-der-Waals solids, layered materials that are currently attracting tremendous attention in the scientific community due to their exciting combination of electrical, optical, and thermal properties. In this context, the present thesis provides predictions and a detailed analysis of the lattice thermal conductivity in Mo and W-based transition metal dichalcogenides. Furthermore, a model is developed to explain the extreme structure sensitivity of the conductivity and calculations are presented that elucidate chemical trends and establish bounds.

The third and fourth paper deal with clathrates, inclusion compounds that have been found to exhibit a combination of transport properties that are very well suited for thermoelectric applications. These materials exhibit extremely small thermal conductivities. The present thesis provides an in-depth analysis of the lat-

tice dynamics of these materials, with a special focus on the thermal conductivity and the so-called phonon-glass behavior.

The present thesis provides a stepping stone for future investigations of transport processes in van-der-Waals solids and clathrates, which eventually should lead to the development of devices with higher energy efficiency and better materials for energy extraction technologies.

Keywords: thermal conductivity, electronic structure calculations, Boltzmann transport theory, phonons, van der Waals solids, layered compounds, clathrates

LIST OF PUBLICATIONS

This thesis consists of an introductory text and the following papers:

I **Microscopic Origin of Thermal Conductivity Reduction in Disordered van der Waals Solids**
Paul Erhart, Per Hyldgaard and Daniel O. Lindroth
Chemistry of Materials **27**, 5511 (2015)

II **Thermal expansion and transport in van der Waals solids**
Daniel O. Lindroth and Paul Erhart
Physical Review B **94**, 115205 (2016)

III **Chemical order and transport properties in an inorganic clathrate: Optimal structures by computational design**
Mattias Ångqvist, Daniel O. Lindroth and Paul Erhart
Chemistry of Materials **28**, 6877 (2016)

IV **Electronic and lattice thermal conductivity in intermetallic clathrates: A first principles perspective**
Daniel O. Lindroth, Erik Fransson, Fredrik Eriksson, Joakim Brorsson, Anders Palmqvist and Paul Erhart
(In preparation)

The author's contributions to the papers:

I The author carried out first principles calculations of phonon spectra and the lattice thermal conductivity.

II The author carried out all of the calculations and was the main author of the manuscript.

III The author carried out the Boltzmann transport calculations.

IV The author carried out the calculations of the lattice contribution to the thermal conductivity and was the main author of the manuscript.

Contents

1 Introduction

1.1 Energy as a resource

It is easy to take energy for granted. At dining tables around the world it is safe to say that the common theme of discussion probably is not the amount of joules needed for enabling the meal at hand. Yet, many joules were spent along the chain from production, to transportation and final preparation.

Energy is such an integral part of our lives that its importance can be hardly overstated, as modern societies are entirely dependent on it. On a personal level for water and food, sanitation, transportation, Internet and communication as well as lighting and heating of our homes. The questions concerning the availability of resources for energy production[1], and their stability over time must be considered among the most important questions for our societies today and in the future.

So, are there any reasons to worry about the available amount of energy in the future? If one compares the total primary energy supply (TPES, An estimate of the available primary energy sources in a region) of the world in 1973 to 2013 the supply has roughly doubled from 6.1 Gtoe (Giga ton of oil equivalent) to 14 Gtoe [2] (Fig. 1.1). At the same time the population has increased from 3.9 to 7.2 billion people, roughly a doubling as well. There is a strong positive correlation between the world population and the global energy consumption. This can be seen when comparing available data for the world population with the global energy consumption in the span from 1980 to 2012 (Fig. 1.2 (a)). Assuming that the world population

[1]Energy production and consumption are here used in the more colloquial sense, not in the sense as a violation of the *first law of thermodynamics* which states that energy cannot be created or destroyed, only transformed from one form to another [1].

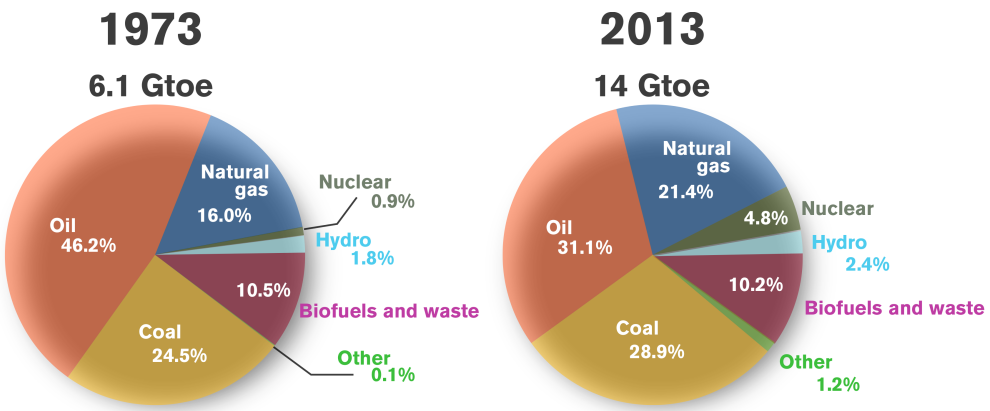

Figure 1.1: Total primary energy supply in the world for different primary energy sources in 1973 and 2013. The data is from the IEA report *Key World Energy Statistics 2015* [2]. The category *Other* includes smaller sources such as geothermal, solar and wind.

is a good estimator for the global energy consumption, up to linear order[2], a linear least squares fit provides a model for estimating the energy consumption based on population size. Using projections of the future world population [4] it is possible to estimate the future energy needs. In a high population scenario the global energy consumption is estimated to steadily increase. Also in a low population scenario the global energy consumption is estimated to increase up until 2050 when it will reach 16 Gtoe after which the demand will start to decline (Fig. 1.2 (b)).

To enable this increase in energy consumption, energy supply must increase as well. In 2013 the global TPES was 81.4 % of the available energy in the form of fossil fuels (coal, oil and natural gas), a small reduction from the 86.2 % in 1973. The oil and gas repositories formed over the last 600 million years [5]. Also coal formed over geological time scales and the fossil fuels are limited resources in that there are finite reserves to extract. Since the reserves are finite the extraction must at some point reach its maximal rate and this sets a physical limit to the possible supply. The point in time where this happens has been coined *the oil peak* [6, 7]. The term *peak* may be used in the context of any type of finite resource and it is reasonable to talk about *peak coal* and *peak gas* besides *peak oil*. Since the contribution of fossil fuel to the TPES is so dominant there is a real concern if the fossil fuels peak without a realistic alternative at hand. According to the estimate

[2]There are some deviations from a linear relation connected to economic cycles and stock market crashes. Following the Black Monday stock market crash of October 1987 [3] there is a pause in the growth of global energy consumption during the following years. Similar, in 2009 there is a violation of the linear trend following the stock market crash of 2008.

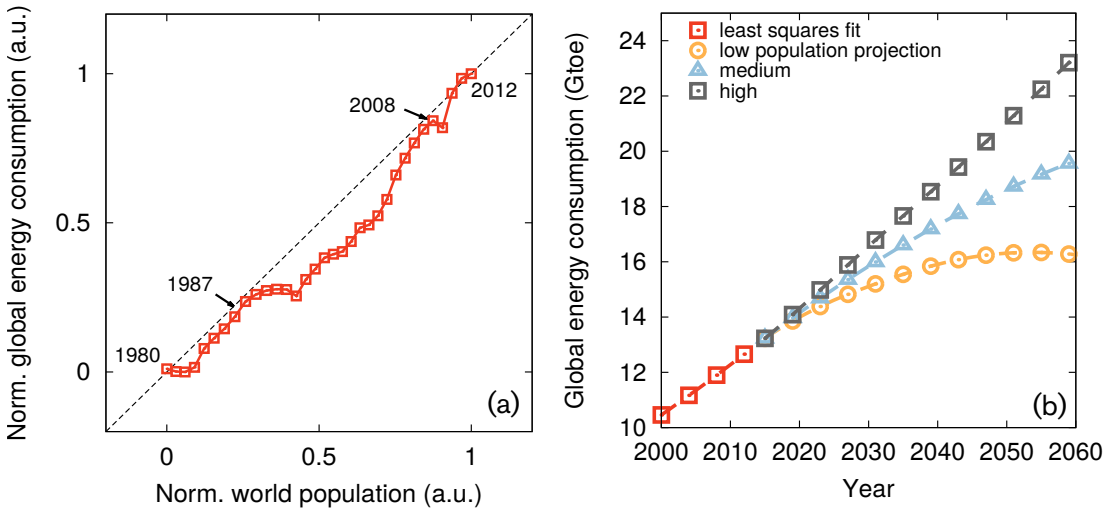

Figure 1.2: (a) Correlation of the world population and yearly total primary energy consumption between the year 1980 and 2011. The data is normalized to the unit interval and received from[4, 10]. (b) Estimations of the future global energy consumption based on three different projections of low, medium and high population growth[4]. The estimates are calculated with a linear model from a least squares fit to the data in the left pane. This gives a connection between yearly energy consumption and the population used in the projections.

the supply necessarily needs to steadily increase. Although debated, claims that the peak of oil is close have been made [8, 9].

There is another concern in the use of fossil fuels as well. The energy source mainly consists of carbon and combustion results in production of carbon dioxide, CO_2, that is deposited into the atmosphere. Carbon dioxide is a so called greenhouse gas in that it is infrared active. The greenhouse gases allow high frequency sunlight to enter the Earth system, heating the ground without any interference. But since the frequencies of the thermal radiation leaving the Earths surface is shifted to the infrared range, some of the radiation will interact with the greenhouse gases and be trapped in the atmosphere. In effect this results in a reduction of the energy flux out of the Earth system resulting in *Global Warming*. The predicted climate change associated with Global Warming is assumed to present a future threat if the emission of CO_2 is not reduced in time to halt the increasing mean temperature of the Earth [11].

The dominating position of fossil fuels in the energy economy makes an exchange of the used resources to alternatives based on the current technologies unrealistic in the near future. And although the power of serendipity can be huge,

it is an unreliable force. Either way, better administration of fossil fuels is a reasonable strategy to handle either fossil peaks or overconsumption resulting in global warming. Increasing the efficiency of energy consumption e.g., by recuperation of waste heat can make a substantial contribution to the solution of this problem.

1.2 Energy transport

Most of the energy we utilize originates from the sun, where fusion of hydrogen releases large amounts of energy that reach the Earth in the form of electromagnetic radiation. On Earth the biosphere assimilates the energy mainly through photosynthesis. Historically a lot of this energy has been stored in the form of fossil fuels (oil, coal and natural gas), which formed as the result of geological processes. Besides the sun, we also utilize energy stored in nuclear fuels and to a lesser extent geothermal energy originating from the Earth's core. Solar, nuclear, and geothermal are examples of primary energy sources, that is energy captured directly from the environment. Secondary forms of energy have been derived from a primary source; this includes for example electricity but also fossil as well as synthetic fuels such as gasoline, ethanol and hydrogen [12].

Electricity is often the most useful form of energy in terms of applications. Several processes can be used for transforming different types of energy into electricity, including e.g., electromagnetic induction, the piezoelectric effect, the photoelectric effect, and the thermoelectric effect. Among these, electromagnetic induction dominates as it is the process used in almost all commercial generation of electricity. With respect to this thesis the thermoelectric effect is very interesting because of its importance of low lattice conductivity for the efficiency in thermoelectric materials [13, 14].

1.2.1 Energy transport as a challenge

The energy stored in fossil fuels can not be used directly, it has to be processed and converted to a form suitable for use. This is a general theme[3] for any kind of utilization of an energy source (Fig. 1.3). There are three fundamental sources of energy [12]. Dominating is energy originating from the sun, followed by nuclear energy and lastly geothermal energy originating from inside the Earth. Fossil fuels originated as energy from the sun accumulating in the biomass from where parts eventually ended up in sedimentary rocks that under the right conditions transformed into coal, oil and gas. To access the stored energy the fuel needs to be

[3] With some exceptions, heating by direct sunlight is one such exception.

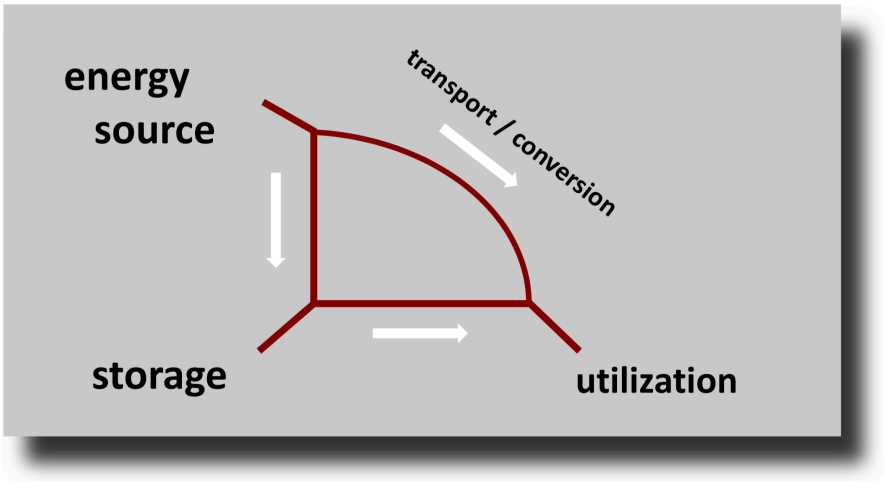

Figure 1.3: After extraction from the energy source it is necessary to store the energy if not directly used. Regardless of the path taken transport processes are present and also one to several types of energy conversion steps.

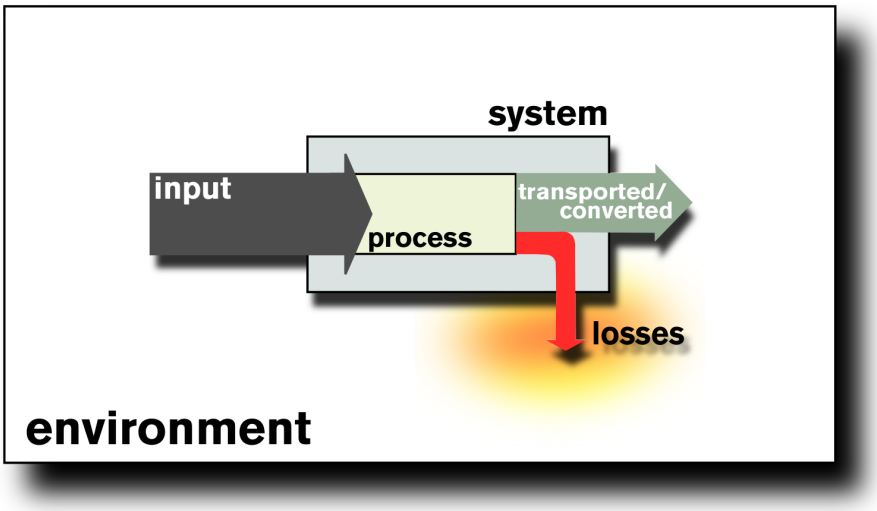

Figure 1.4: Schematics of energy interacting with a system. The energy input is converted and transported through a redirection resulting in useful energy output of transported/converted energy. At the same time, inevitably energy is dissipated to the surrounding environment due to irreversible processes within the system.

combusted and further transformed into a useful form e.g., electricity or mechanical work.

In any type of process involving energy transport or conversion there will be energy dissipation to internal degrees of freedom due to irreversibility [15, 16]. This dissipation will eventually transfer into the surrounding environment resulting in energy losses (Fig. 1.4). The result is a degradation of the energy used as input. For thermal processes these losses are substantial. The disadvantage with dissipated energy is its disordered nature with no clear direction. This makes utilization difficult.

1.2.2 Scavenging (waste) heat

Because of the dominating position of thermal processes in the economy, technologies that scavenge dissipated energy and thereby raise the overall energy efficiency are of great interest.

Heat engines convert heat into useful, most commonly mechanical or electrical, energy. A specific type of heat engine is the thermoelectric generator (TEG) [13], which converts heat into electrical current by exploiting the thermoelectric effect. The efficiency is here dependent on several factors, one of which is the thermal conductivity with lower values providing better efficiency. To make TEGs economically feasible the efficiency needs to be high enough, higher than it is today. Because of this an understanding how to engineer the thermal conductivity is important.

At the same time, knowledge about how to lower the conductivity can be used to achieve the opposite, namely increasing the conductivity. This has important implications for heat management in devices. In particular, a high thermal conductivity is important for applications in electronics and opto-electronics to prevent overheating and potential loss of components.

2 Background

2.1 Overview

Thermal transport and conversion can quantitatively be understood from either the macroscopic or the microscopic perspective. Macroscopic theories regarding energy transport are within the field of thermodynamics for systems out of equilibrium. In section 2.2 is non-equilibrium thermodynamics introduced. The notion of entropy in a non-equilibrium setting is discussed, together with its relation to thermodynamic forces and fluxes in the case of thermal and charge imbalance. The corresponding phenomenological laws with the Onsager coefficients are then introduced, together with the relations for the electrical and thermal conductivity, as well as the Seebeck and Peltier coefficients. Because of the close relation to non-equilibrium thermodynamics, and the potential role in heat recuperation, the section ends with an introduction to thermoelectric generation and efficiency, together with the concept of the thermoelectric figure-of-merit.

The following section 2.3, takes a qualitatively look on thermal transport from the kinetic point of view. An estimate for the thermal conductivity is derived by the introduction of a mean free path, mean velocity and specific heat for fluxes of particles in a temperature gradient, while connecting the energy flux with the temperature gradient through Fourier's law.

Section 2.4 introduces quantitative microscopic transport theory through Boltzmann transport theory for both electrons and phonons. The relaxation time approximation is introduced together with a discussion of lifetimes.

Finally, section 2.5 introduces the two classes of material of interest, van der Waals solids and inorganic clathrates.

2.2 Non-equilibrium thermodynamics

Tracing all degrees of freedom on the atomic scale is all but tractable since the number of constituents in an analysis of everyday objects typically is of the order 10^{23}. The pragmatic stance is to look for and analyze properties where the degrees of freedom collectively average into macroscopically observable effects, including time- as well as spatial averaging.

In general, classical thermodynamics is the study of the macroscopic properties of systems in *equilibrium*. When in equilibrium, the macroscopic properties are both static and spatially homogeneous, i.e., they do not vary with time and remains constant over the extent of the system. The macroscopic properties are used as state variables, i.e., macroscopic variables that as a set uniquely define the equilibrium state of the system.

One obvious limitation of this description is the lack of time-dependence. In reality, systems can change states from one instant to another. A hot cup of coffee left on the desk is out of equilibrium, it will continuously lose energy through heat until reaching the equilibrium temperature of its surroundings. The end of this process is naturally called the *final state* of the cooling process. Further, assuming spatial homogeneity, one can imagine the beginning of this cooling process as being released from another equilibrium state at a higher temperature, then called the *initial state*. Classical thermodynamics here brackets the cooling process but gives little insight into the actual progression of the cooling. When regarding change within the context of classical thermodynamics, at best, one can view the system as changing from one equilibrium state into another, without departure from the continuum of equilibria. One prerequisite for such evolution is that the transition between states is slow enough, even infinitesimally slow to ensure that the system never leaves equilibrium. Such a process is then called *quasi-static*. At best, this would be an approximation of the real change, and as important, it says nothing about real rates.

A *reversible process* is by definition a quasi-static process, such that both the system and its surroundings go back to the original states if the process is reversed. Such requirements rule out the previous example of cooling. Since cooling is the process of losing energy to the surroundings through heat, the process reversed would be the surroundings losing energy to the coffee through heat. For such reversal, the ambient temperature needs to be higher than the temperature of the coffee, all the way up to the temperature at the initial state. A process that is not reversible is called *irreversible* and includes quasi-static processes that are not reversible, as well as processes that evolve in finite time.

In contrast to the limitations due to lack of dynamics in classical thermodynam-

ics,[1] *non-equilibrium thermodynamics* concerns the study of systems with macroscopic properties subject to time-dependence as well as spatial variations. This time-dependence essentially makes non-equilibrium thermodynamics to be of an irreversible nature, and the general theory is interchangeably referred to as *irreversible thermodynamics*.

In practice, to treat irreversible systems, the most common approach is suitable when processes responsible for internal equilibration occur on time-scales much shorter than the time-scale for macroscopic change in the state variables. It is then possible to evoke the *local-equilibrium hypothesis*. The hypothesis postulates that the total system in question can be artificially divided into subsystems, in such a way that each sub-system is effectively in equilibrium, and can be treated as a macroscopic thermodynamic system. The advantage is that classical thermodynamics is valid within each sub-system and all thermodynamic variables are locally well defined, including entropy and temperature. The hypothesis further assumes that the equilibrium state in a sub-system can change in time due to interactions with neighboring sub-systems and that the state variables can be assumed to be continuously dependent on time and spatial coordinates. In this thesis, the focus will be on systems where the local-equilibrium hypothesis is assumed to be valid.

2.2.1 Entropy and the second law of thermodynamics

In classical thermodynamics, entropy has a central role due to the second law of thermodynamics, which states that the total entropy in a closed system always increases. From a macroscopic perspective when concerned with thermal interactions, the entropy S in thermodynamics is naturally defined as the state function related to the exact differential one obtains after dividing the inexact differential of added heat δQ with the system temperature T, which gives the relation $\mathrm{d}S = \delta Q/T$. Hence, entropy depends on the temperature being a well-defined quantity. For a system out of equilibrium, the assumption of a local-equilibrium provides a bridge to definitions of entropy in systems out of equilibrium.

The validity of the local-equilibrium hypothesis implies that the description of local state variables in equilibrium is valid even when the full system is out of equilibrium. The hypothesis enables a definition of entropy for a system out of equilibrium in such a way that the out of equilibrium entropy depends on the same state variables as for the system in equilibrium. The specific entropy, defined as the entropy per unit mass, is then a continuous function in space and time. When the system is described as a fluid of N different components, the specific entropy is a function of the specific energy u, specific volume v, as well as the mass fractions

[1] One can argue that thermodynamics, in this regard is an unfortunate name, *thermostatics* would be more proper. However, as for now, the name is cemented into the subject.

c_j of species j

$$s(\boldsymbol{r}, r) = s[u(\boldsymbol{r}, t), v(\boldsymbol{r}, t), c_1(\boldsymbol{r}, t), \ldots, c_N(\boldsymbol{r}, t)]. \tag{2.1}$$

In the absence of convective transport, the equivalent differential form is

$$\mathrm{d}s = \left(\frac{\partial s}{\partial u}\right)_{v,c_k} \mathrm{d}u + \left(\frac{\partial s}{\partial v}\right)_{u,c_k} \mathrm{d}v + \sum_{j\neq k}^{N} \left(\frac{\partial s}{\partial c_k}\right)_{u,v,c_j} \mathrm{d}c_k, \tag{2.2}$$

where the expansion coefficients are defined as $1/T$, p/T and μ_k/T respectively. Here, T is the temperature, p the pressure and μ_k the chemical potential for particle species k. With these quantities defined, we have the following equation

$$\mathrm{d}s = \frac{1}{T}\mathrm{d}u + \frac{p}{T}\mathrm{d}v - \sum_{k=1}^{N} \frac{\mu_k}{T}\mathrm{d}c_k. \tag{2.3}$$

When the local equilibrium hypothesis holds, the intensive parameters are effectively in equilibrium on the macroscopic scale. Still, there is a macroscopic evolution dependent on local interactions between subsystems. The time evolution of the specific entropy is directly expressed through the time derivative of Eq. (2.3)

$$\frac{\mathrm{d}s}{\mathrm{d}t} = \frac{1}{T}\frac{\mathrm{d}u}{\mathrm{d}t} + \frac{p}{T}\frac{\mathrm{d}v}{\mathrm{d}t} - \sum_{k=1}^{N} \frac{\mu_k}{T}\frac{\mathrm{d}c_k}{\mathrm{d}t}. \tag{2.4}$$

This equation is central in the theory, since it is used for identification of entropy production. Using conservation laws for the total energy balance, total mass balance, as well as mass fraction balance, Eq. (2.4) is a general statement determining the time evolution of the specific entropy. As discussed in appendix A.2, the equation for local entropy balance is

$$\rho\frac{\mathrm{d}s}{\mathrm{d}t} = -\nabla \cdot \boldsymbol{J}_s + \sigma_s, \tag{2.5}$$

where the entropy flux $\boldsymbol{J}_s$ originates from thermodynamic imbalance to neighboring systems, and the entropy production term is subject to a local constraint $\sigma_s \geq 0$.

2.2.2 Thermodynamic forces and fluxes

When there is a temperature difference in a system, the response is an energy flux with an equilibrating effect on the temperature difference. This equilibration is

associated with heat transport through a heat flux $\boldsymbol{J}_q$. Assuming a linear response, the phenomenological law for heat conduction, Fourier's law, is written as

$$\boldsymbol{J}_q = -\kappa \nabla T, \tag{2.6}$$

where the proportionality tensor κ is known as the thermal conductivity. When entropy is a dependent quantity, the entropic representation is more suitable, in which case Fourier's law is expressed through [2]

$$\boldsymbol{J}_q = \kappa T^2 \nabla \frac{1}{T}. \tag{2.7}$$

The gradient of the inverse of the temperature field acts as the cause, producing the effect of a heat current. It is natural to interpret this cause as a thermodynamic force. When there is no volume change or exchange of matter, Eq. (2.3) reduces to

$$T \frac{\mathrm{d}s}{\mathrm{d}t} = \frac{\mathrm{d}u}{\mathrm{d}t}. \tag{2.8}$$

With the use of the corresponding balance equation for the internal energy

$$\rho \frac{\mathrm{d}u}{\mathrm{d}t} = -\nabla \cdot \boldsymbol{J}_q, \tag{2.9}$$

and Eq. (2.5) for entropy balance, the entropy production associated with heat conduction is

$$\sigma_s^q = \boldsymbol{J}_q \cdot \nabla \frac{1}{T}, \tag{2.10}$$

given that the entropy flow is defined through the heat flow

$$\boldsymbol{J}_s = \frac{\boldsymbol{J}_q}{T}, \tag{2.11}$$

in analogy with classical thermodynamics. The entropy production term is in the form of a flux multiplied by the corresponding thermodynamic force.

If a system is at a constant temperature but has a difference in the electrochemical potential due to an external potential $\varphi = \mu/e$, an electric current flows through the system. According to Ohm's law, the electric current $e\boldsymbol{J}_n$ [3], defined as the particle flux times the elementary charge, is the effect of the external potential acting as a force

$$e\boldsymbol{J}_n = -\sigma \cdot \nabla \varphi, \tag{2.12}$$

[2] Using the identity $\frac{\partial}{\partial x}\frac{1}{T} = -T^{-2}\frac{\partial T}{\partial x}$.

[3] The electrical current is here defined so that the direction of positive charge carriers corresponds to a positive current.

where σ is the electrical conductivity tensor. Following a treatment similar to the case of heat flow, with the addition of charge/mass conservation, the entropy flux is

$$\boldsymbol{J}_s = \frac{\varphi}{T} e\boldsymbol{J}_n = \frac{\mu}{T}\boldsymbol{J}_n, \tag{2.13}$$

The entropy production is then

$$\sigma_s = -\frac{1}{T}\nabla\left(\frac{\mu}{e}\right)\cdot\left(-e\boldsymbol{J}_n\right) = \frac{1}{T}\nabla\mu\cdot\boldsymbol{J}_n. \tag{2.14}$$

The entropy production is here associated with potential energy transforming into heat.

If both the temperature and the electrochemical potential varies in the system, the heat flux and the electrical current couples. Assume the system operates under steady state, so that any time dependence vanish. For the coupled system, define a total energy density current $\boldsymbol{J}_u$, a particle current $\boldsymbol{J}_n$ and an entropy current $\boldsymbol{J}_s$. Both the total energy current and the particle current is source free, and must therefore be divergence free, i.e., both $\nabla\cdot\boldsymbol{J}_u$ and $\nabla\cdot\boldsymbol{J}_n$ are equal to zero. The entropy on the other hand is not source free, and has source term σ_s, so that $\nabla\cdot\boldsymbol{J}_s = \sigma_s$. From the corresponding balance equations, Eq. (2.3) gives a relation between the fluxes

$$T\boldsymbol{J}_s = \boldsymbol{J}_u - \mu\boldsymbol{J}_n. \tag{2.15}$$

By taking the divergence of this relation, using that the total energy and the particle current is source free, gives the entropy production as

$$\sigma_s = \nabla\cdot\boldsymbol{J}_s = \nabla\frac{1}{T}\cdot\boldsymbol{J}_u - \nabla\frac{\mu}{T}\cdot\boldsymbol{J}_n. \tag{2.16}$$

Define the heat current as $\boldsymbol{J}_q = T\boldsymbol{J}_s$, then Eq. (2.15) gives the heat flux as

$$\boldsymbol{J}_q = \boldsymbol{J}_u - \mu\boldsymbol{J}_n. \tag{2.17}$$

This definition agrees with the intuition of heat as the difference between the total energy and energy related to external energy. The divergence of this expression gives the relation

$$\nabla\cdot\boldsymbol{J}_q = -\nabla\mu\cdot\boldsymbol{J}_n, \tag{2.18}$$

that is, increase in the heat current corresponds to the decrease in the potential energy flux, the potential energy converts into heat. Expressing the entropy production with the use of heat flux gives

$$\sigma_s = \nabla\frac{1}{T}\cdot\boldsymbol{J}_q - \frac{1}{T}\nabla\mu\cdot\boldsymbol{J}_n. \tag{2.19}$$

Using Eq. (2.18) the entropy production can be expressed in a symmetric form

$$\sigma_s = \nabla\frac{1}{T}\cdot \boldsymbol{J}_q + \frac{1}{T}\nabla\cdot \boldsymbol{J}_q, \tag{2.20}$$

showing that the entropy production in part is due to heat transfer caused by a temperature gradient, and part from dispersion of potential energy into heat.

2.2.3 Phenomenological laws and transport coefficients

In general, assuming linear coupling, each flux component can be expanded with phenomenological constants multiplying the corresponding thermodynamic forces causing the fluxes. The phenomenological constants are then to be determined either by experiment or by microscopic theory. The coupling between flux components and the thermodynamics forces F_j are expressed through the relations

$$J_i = \sum_j L_{ij}F_j. \tag{2.21}$$

The phenomenological coefficients L_{ij} are also known as Onsager coefficients or kinetic coefficients. As shown by Onsager, the off-diagonal coefficients fulfill a symmetry condition $L_{ij} = L_{ji}$ when the system is microscopically reversible as a result of the time reversal invariance of physical laws. When the entropy production is stated as the sum of flux and force pairs, using the Onsager coefficients, the entropy production is

$$\sigma_s = \sum_i J_i F_i = \sum_{i,j} F_i L_{ij} F_j \geq 0. \tag{2.22}$$

In the case of coupled heat and electron transfer, the phenomenological equations are

$$-\boldsymbol{J}_n = L_{11}\frac{1}{T}\nabla\mu + L_{12}\nabla\frac{1}{T}, \tag{2.23}$$

$$\boldsymbol{J}_q = L_{21}\frac{1}{T}\nabla\mu + L_{22}\nabla\frac{1}{T}, \tag{2.24}$$

when the fluxes are chosen as the heat flux and the particle flux. [4]

Ohm's law states that the electrical conductivity is the ratio between the electric current and the gradient of the chemical potential at thermal equilibrium. Solving

[4] To simplify, it is here assumed that the system is isotropic, so that each type of Onsager coefficient can be represented with a single value instead of a second rank tensor.

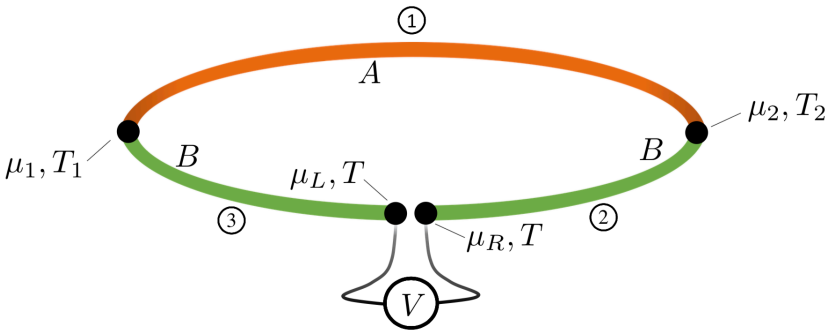

Figure 2.1: Schematic of a thermocouple consisting of joined materials A and B, probed with an ideal voltage meter. The junctions are assumed to be maintained at temperatures T_1 and T_2, resulting in the build-up of an electrochemical potential μ. The voltmeter is assumed to block the charge current, while fully permitting heat to flow so that the temperature is the same on both the immediate left and right side of the voltmeter.

for the ratio $-e\boldsymbol{J}_n/\nabla(\mu/e)$ when $\nabla(1/T) = 0$ in the first phenomenological equation, directly gives the electrical conductivity σ as

$$\sigma = e^2 \frac{L_{11}}{T}. \tag{2.25}$$

The thermal conductivity varies with temperature through an explicit factor of $1/T$. Inverting the expression gives the first Onsager coefficient as

$$L_{11} = \frac{\sigma}{e^2} T, \tag{2.26}$$

expressed through measurable properties.

According to Fourier's law, the thermal conductivity is the heat current per unit thermal gradient when there is no particle current. Assuming $\boldsymbol{J}_n = 0$, solving for the ratio $-\boldsymbol{J}_q/\nabla T$ in the phenomenological equations, while making use of the reciprocity $L_{12} = L_{21}$, gives the thermal conductivity κ expressed in Onsager coefficients and the temperature

$$\kappa = \frac{L_{11}L_{22} - L_{12}^2}{L_{11}T^2}. \tag{2.27}$$

Showing that the thermal conductivity should have a temperature dependence with an explicit factor of $1/T^2$.

The phenomenological equations can also be applied to a thermocouple (Fig. 2.1). A thermocouple consists of two different conductors or semiconductors,

joined at each end. Keeping each junction at different temperatures induces charge carrier diffusion in the system and the build-up of a chemical potential. Assume an idealized voltage meter inserted into one of the legs of the thermocouple. The voltage meter is assumed to block passage of electric current, while freely allowing heat to flow. The electrochemical potential will then be different on each side of the voltage meter, while the temperature will be the same. When there is no current, i.e., $\boldsymbol{J}_n = 0$, the first phenomenological equation gives the relation

$$\nabla\mu = \frac{L_{12}}{L_{11}T}\nabla T. \tag{2.28}$$

This equation can be solved along three different paths, one over the material A, as well as the two separate parts in material B, separated by the volt meter (Marked as 1, 2 and 3 in Fig. 2.1), which gives the system of equations

$$\mu_2 - \mu_1 = \int_{T_1}^{T_2} \frac{L_{12,A}}{TL_{11,A}}\,\mathrm{d}T, \tag{2.29}$$

$$\mu_2 - \mu_L = \int_{T}^{T_2} \frac{L_{12,B}}{TL_{11,B}}\,\mathrm{d}T, \tag{2.30}$$

$$\mu_R - \mu_1 = \int_{T_1}^{T} \frac{L_{12,B}}{TL_{11,B}}\,\mathrm{d}T. \tag{2.31}$$

These equations can be solved for the potential V over the voltage meter by eliminating μ_1 and μ_2

$$V = \frac{\mu_R - \mu_L}{e} = \int_{T_1}^{T_2} \left(\frac{L_{12,A}}{eTL_{11,A}} - \frac{L_{12,B}}{eTL_{11,B}} \right) \mathrm{d}T. \tag{2.32}$$

Defining the absolute Seebeck coefficient for material A as

$$\alpha_A = -\frac{L_{12,A}}{eTL_{11,A}}, \tag{2.33}$$

and define α_B similarly for material B, gives the Seebeck coefficient for the thermocouple as

$$\alpha_{AB} = \alpha_B - \alpha_A. \tag{2.34}$$

The sign in Eq. (2.33) is chosen such that an increase in α_{AB} corresponds to a particle current in the A to B direction at the hotter junction. With the use of Eq. (2.26) the L_{12} coefficient is expressed through physical parameters

$$L_{12} = -\alpha eTL_{11} = -\frac{\alpha\sigma T^2}{e}. \tag{2.35}$$

With expressions for L_{12} and L_{11}, the L_{22} coefficient in Eq. (2.27) can be solved for

$$L_{22} = \alpha^2 \sigma T^3 + \kappa T^2. \tag{2.36}$$

With L_{11}, L_{12} and L_{22} determined, it is now possible to express the entropy flux in terms of measurable quantities

$$\boldsymbol{J}_s = \alpha e \boldsymbol{J}_n + \kappa T \nabla \frac{1}{T}. \tag{2.37}$$

This expression presents a physical interpretation of the Seebeck coefficient, as the amount of entropy transported by each charge carrier in the charge carrier flux. This is an additional contribution to the entropy flux, compared to the decoupled entropy current that is directly associated with the heat current $\boldsymbol{J}_q$.

In the special case of charge carrier flux under isothermal conditions, the heat flux in the phenomenological equation, Eq. (2.24), can be solved in terms of measurable quantities

$$\boldsymbol{J}_q = \alpha T e \boldsymbol{J}_n. \tag{2.38}$$

If this flux is within a thermocouple, over a junction from material A to material B, the difference in heat current over the junction has to be discontinuous by an amount

$$\Delta Q_{AB} = \boldsymbol{J}_{q,B} - \boldsymbol{J}_{q,A} = (\alpha_B - \alpha_A) T e \boldsymbol{J}_n = \alpha_{AB} T e \boldsymbol{J}_n. \tag{2.39}$$

The Peltier coefficient, denoted π_{AB}, is now defined as the amount of heat per unit current that must be supplied, or dissipated, at the junction

$$\pi_{AB} = \frac{\Delta Q_{AB}}{e \boldsymbol{J}_n} = \alpha_{AB} T. \tag{2.40}$$

This shows that the Peltier- and Seebeck coefficients are dependent to each other, related by a factor of T. The two physical effects are not independent. The Seebeck effect corresponds to thermoelectric a transformation of heat flow into an electromotive force. The Peltier effect is the process in reverse, transformation of electric energy into external heat flow.

2.2.4 Thermoelectric generation and thermodynamic efficiency

A heat engine operates under the working principle of transporting thermal energy from a heat source into the engine consisting of some thermodynamic substance

capable of converting part of the transported energy into power output. The working substance then rejects the excess energy to a colder reservoir. This rejection is necessary which can be understood by considering a heat engine working in cycles. Along with the thermal energy transported, there is an influx of entropy to the working substance. If the engine is irreversible, there is also entropy produced in the conversion process. For the thermodynamic system to go back to the original state of the cycle, entropy must leave the system, usually by transport of heat to the heat sink.

The efficiency η of the energy conversion is defined as the ratio between the energy transformed into work and the energy supplied to the heat engine. For an idealized reversible heat engine there is no entropy produced and therefore characterizes the maximal efficiency achievable by a heat engine. The efficiency of a reversible heat engine is called the Carnot efficiency and is only dependent on the temperature of the energy source T_H and the temperature of the reservoir for heat rejection T_C, such that

$$\eta_{Carnot} = 1 - \frac{T_C}{T_H}. \tag{2.41}$$

For real heat engines the production of entropy further reduces the efficiency by some factor. The factor

$$\gamma = \frac{\eta}{\eta_{Carnot}} \tag{2.42}$$

is then a measure of the deviation from an ideal heat engine, and the value of γ is one important factor when choosing an engine for real applications.

The thermoelectric generator constitutes a specific class of heat engines. The basic unit in the generator is two semiconductors, one of n-type and the other of p-type, joined by a conductor at the hotter side to form a thermocouple. At the colder side, external conductors are attached to the thermocouple (Left panel in Fig. 2.2) allowing for charge carrier diffusion, with the effect of increasing electrostatic potential between the attached wires. The n-type semiconductor has a negative Seebeck coefficient resulting in electrons being diffused from the hotter side to the colder side. In the p-type semiconductor the Seebeck coefficient is positive, so that electron holes is the charge carrier diffusing to the colder side. Closing the circuit over an electric load results in an electric current powering the load, as long as there is a thermal difference maintained over the thermocouple.

A large thermopower together with a high capability of charge conduction and ability to maintain a thermal gradient is essential for an efficient thermoelectric generator. High thermopower strengthens the coupling between heat and the charge carrier current, a large electric conductivity reduces energy losses due to Joule heating, and low thermal conductivity ensures that the thermal gradient

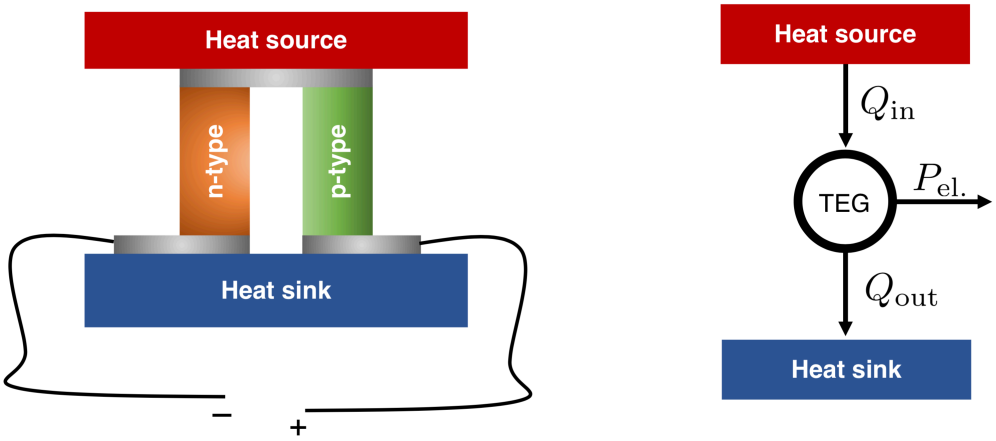

Figure 2.2: The left panel shows the schematics of a basic thermoelectric generator consisting of a thermocouple with legs out of an n-type semiconductor and a p-type semiconductor. The Semiconductors are directly joined by a conductor at the hotter end. At the colder end conducting wires are attached to each leg. The right panel shows the schematics of a thermoelectric generator (TEG) as a heat engine. The generator absorbs heat Q_{in} at the hotter end, converts a portion of Q_{in} to electric power $P_{el.}$, and disposes excessive heat Q_{out} to the heat sink.

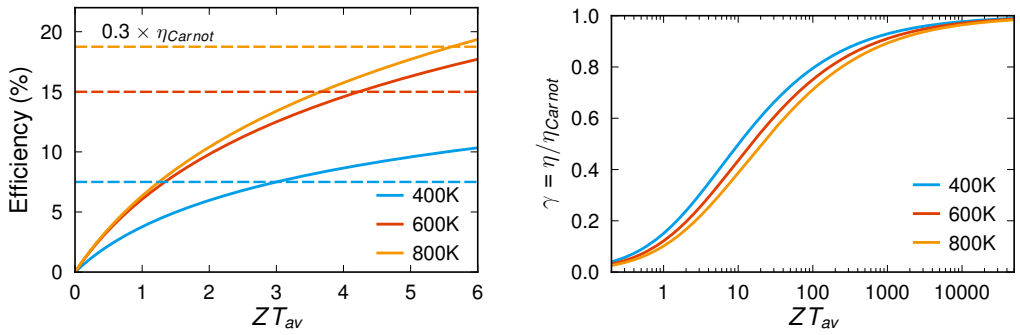

Figure 2.3: The left panel shows the thermodynamic efficiency η (solid lines) for a thermoelectric generator operating at three different temperatures relative a heat sink at 300K. The vertical dashed lines show the efficiency for heat engines operating at 30% of the Carnot efficiency at the same set of working temperatures. The right panel shows the reduced efficiency factor γ for the same temperature differences as in the left panel.

sustains. By formulating a dimensionless parameter, the thermoelectric figure of merit zT, a first measure of a materials suitability for thermoelectric applications is given as

$$zT = \frac{\alpha^2 \sigma}{\kappa} T. \tag{2.43}$$

To estimate the efficiency of a thermoelectric generator the ratio between the power output $P_{el.}$ and the heat absorbed from the heat source Q_{in} is formed (Fig. 2.2). With the use of the phenomenological expressions for the charge current and the heat current an expression for the reduced efficiency factor γ is derived

$$\gamma = \frac{\sqrt{1 + ZT_{av}} - 1}{\sqrt{1 + ZT_{av}} + T_C/T_H}. \tag{2.44}$$

Here, T_{av} is the average temperature of the heat source and the cooler reservoir, and ZT a figure of merit suitable when two materials are combined into a thermocouple

$$ZT = \frac{(\alpha_p - \alpha_n)^2 T}{\left(\sqrt{\kappa_n/\sigma_n} + \sqrt{\kappa_p/\sigma_p}\right)^2}. \tag{2.45}$$

Even though the material parameters in general are temperature dependent, the use of average values should produce values of ZT that are within 10% of the true ZT values [17]. In the theoretical limit of really high ZTs, the factor γ approaches one, and with that the efficiency approaches the Carnot efficiency (Right panel, Fig. 2.3).

When comparing the reduced efficiency for a thermoelectric generator, to the efficiency of other heat engines, it is seen that a thermoelectric generator with a ZT above three starts to become competitive to heat engines operating at 30% of the full Carnot efficiency (Left panel Fig. 2.3). Today, realistic values of ZT values is about one, a factor of three from being competitive with other technologies, efficiency considered. At the same time, others factors than the efficiency can be crucial for how suitable the technology is. Thermoelectric generators have attractive properties in that they are silent, reliable and scalable. These set of properties makes thermoelectric generators ideal for small-scale distributed power generation, for instance in remote locations [13].

2.3 Transport theory

Materials and their ability to transfer charge (electrical currents) and heat (thermal currents) play a key role in energy management as they are essential compo-

nents in energy extraction, transport, storage, and consumption technologies. On a macroscopic level electrical and thermal conduction in a material can be conveniently described using phenomenological theories e.g., in the form of Ohm's law in the case of electrical conduction and Fourier's law in the case of thermal conduction (see below). The corresponding equations contain transport coefficients such as the electrical conductivity, the Seebeck coefficient, or the thermal conductivity. These are tensorial quantities that are material specific and quantify the response to an external force such as an electric field or a thermal gradient[18].

For example, the thermal conductivity can be phenomenologically defined through Fourier's law

$$\boldsymbol{J} = -\kappa \cdot \nabla T, \tag{2.46}$$

where $\boldsymbol{J}$ is the heat current, which quantifies the rate at which thermal energy is transported as the result of a thermal gradient ∇T, and κ denotes the thermal conductivity tensor.

It is illuminating to examine thermal conductivity from a kinetic point of view as a transport problem in a monatomic gas. To this end, let us assume a stationary thermal gradient in the x-direction. When a particle moves from a region at temperature $T + \Delta T$ to a colder region at temperature T where it thermalizes it needs to give up an energy of $C\Delta T$ from the hotter region to equilibrate, where C is the specific heat. The particle will now be in thermal contact with the new region. Assuming that the length scale for thermalization is ℓ (Fig. 2.4), the expression for the temperature difference is

$$\Delta T = \ell \frac{\partial T}{\partial x}. \tag{2.47}$$

The thermal energy is proportional to the temperature $E \sim T$ and the mean velocity squared $E \sim v^2$. Hence, the mean velocity is proportional to the square root of the temperature and the mean velocity at temperature $T + \Delta T$ is

$$v \sim \sqrt{T + \Delta T} = \sqrt{T}\sqrt{1 + \frac{\Delta T}{T}} \approx \sqrt{T}\left(1 + \frac{1}{2}\frac{\Delta T}{T}\right) = \sqrt{T} + \frac{1}{2}\frac{\Delta T}{\sqrt{T}}. \tag{2.48}$$

For relatively small ΔT the mean velocities are therefore the same.

The particle flux per unit area is given by the mean velocity multiplied with the particle density. The energy flux is then the particle flux multiplied by the average energy ε the particles in the stream are transporting. Over a mean free path ℓ there will be a ballistic transport in both directions. The net flux over the middle

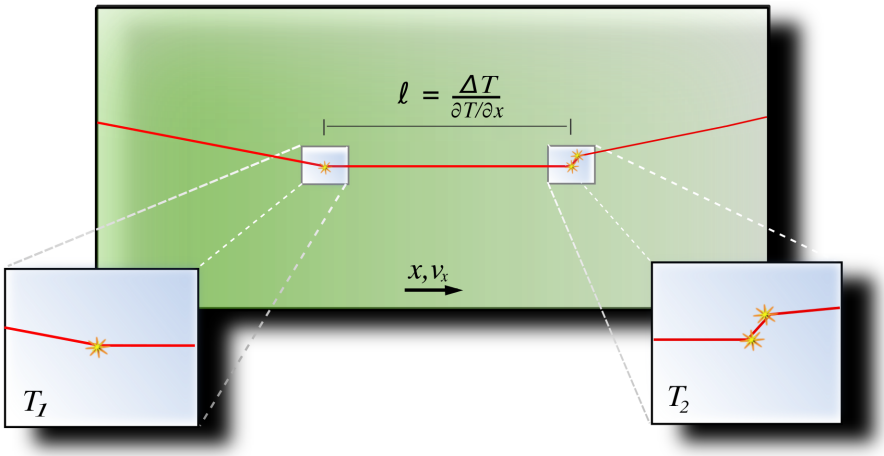

Figure 2.4: The physical picture of the mean free path ℓ in kinetic theory as the length scale between thermalization of a particle propagating in a thermal gradient field.

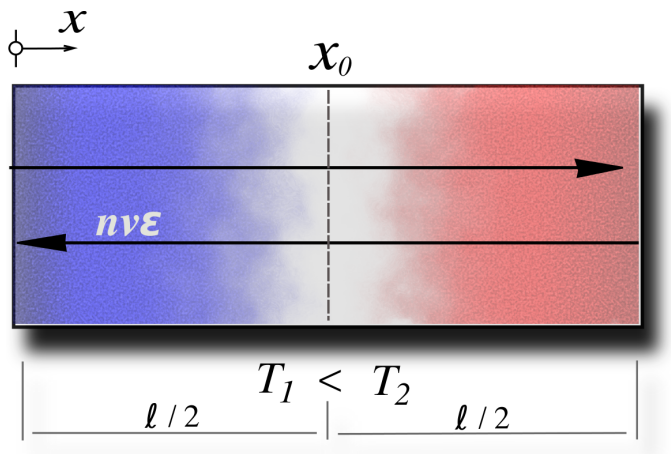

Figure 2.5: The heat flux at x_0 is the net energy flux resulting from ballistic transport over the mean free path ℓ in both directions.

of ℓ (Fig. 2.5) is then

$$J = \frac{1}{2} n v \varepsilon \big|_{x_0 - \ell/2} - \frac{1}{2} n v \varepsilon \big|_{x_0 + \ell/2} = \frac{1}{2} v \varepsilon \big(n(x_0 - \ell/2) - n(x_0 + \ell/2) \big)$$
$$\approx -\frac{1}{2} v \varepsilon \frac{\mathrm{d}n}{\mathrm{d}x} \ell = -\frac{1}{2} v \ell \frac{\mathrm{d}}{\mathrm{d}T}(\varepsilon n) \frac{\mathrm{d}T}{\mathrm{d}x} = -\frac{1}{2} v \ell c \frac{\mathrm{d}T}{\mathrm{d}x}, \tag{2.49}$$

where c denotes the specific heat per unit volume. An estimate for the thermal conductivity can then be identified from Fourier's law as

$$\kappa \sim v \ell c. \tag{2.50}$$

This illustrates that the thermal conductivity ought to depend on the mean velocity with which the energy is transported, the length scale for that transport without inelastic scattering as well as the average energy that a carrier transfers.

In this derivation we implicitly assumed local equilibration such that a thermal gradient can be established. This shows that heat is transported downhill with respect to the thermal gradient in accordance with the second law of thermodynamics as stated by Clausius[1]:

No process is possible whose sole result is the transfer of heat from a colder to a hotter body.

For two regions that are thermally connected there will thus always be heat transfer from the hotter to the colder side, unless there is an additional process reversing the heat current.

Equation Eq. (2.50) was derived for a gas of classical particles but can be used to understand the thermal conductivity in solids as well. The heat carriers in solids are electrons and phonons, and the picture above can be adapted by observing that both of these quasi-particles behave as quantum gases for which the correct statistics have to be used.[5]

2.4 Boltzmann transport theory

The book keeping associated with tracking the dynamical variables in one mole of substance is an infeasible task. One attempt at a remedy is to severely reduce the system size, impose suitable boundary conditions and see if this reduction still manages to capture the relevant physics. If this does not work or becomes to difficult an alternative strategy is to abandon exact knowledge of the system and instead give a statistical description. For mechanical systems the concept of distribution functions that tracks the number density over phase space is useful.

[5] For electrons, which are fermions, Fermi-Dirac statistics apply, whereas phonon as bosons obey Bose-Einstein statistics.

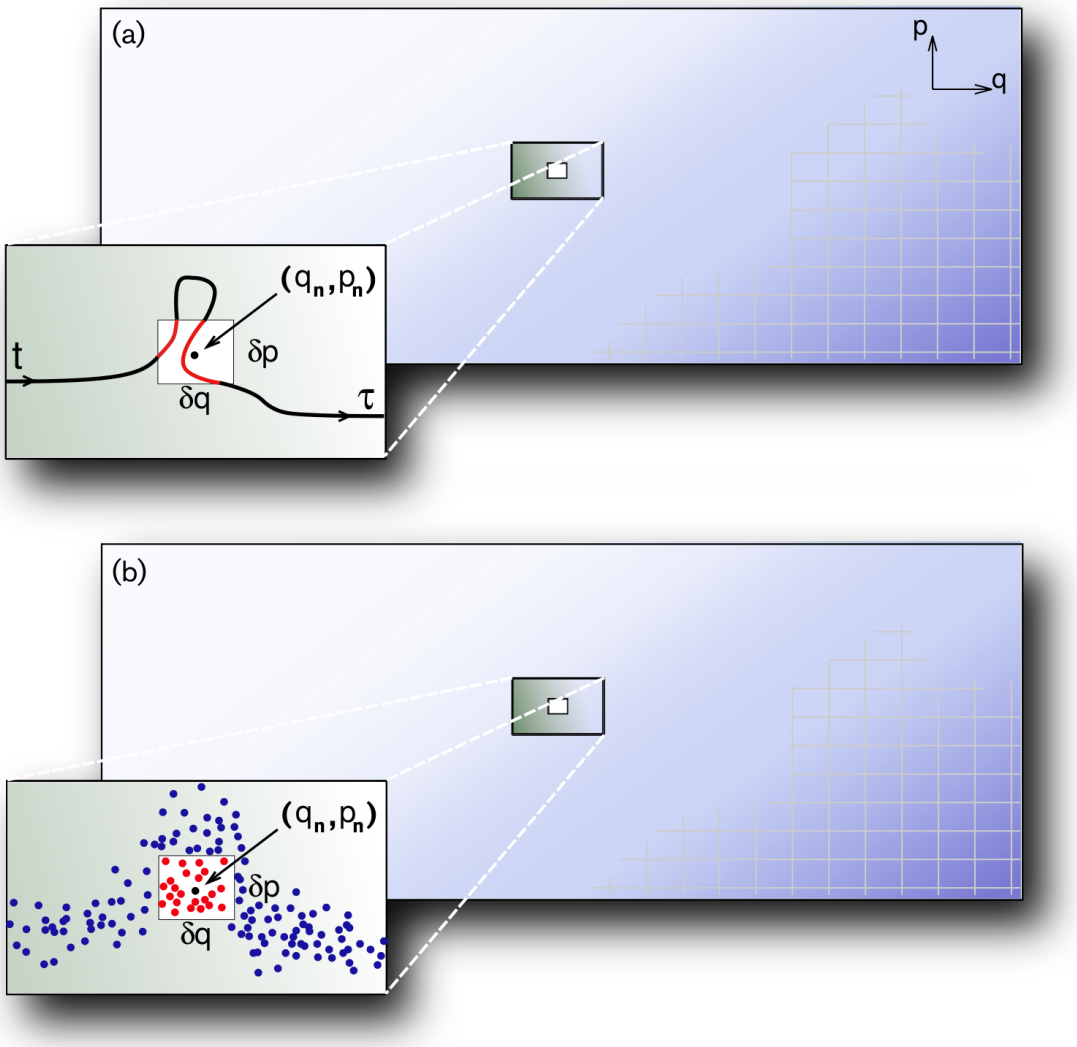

Figure 2.6: Schematic representation of two different views on distribution densities over phase space. (a) Tracking the amount of time a system spends in the neighborhood of a specific phase space point (the red paths) gives a measure for a distribution function. (b) A large enough collection of independent system replicas gives an alternative measure for a distribution function as the ratio between states within a neighborhood to $(\boldsymbol{q}, \boldsymbol{p})$ and all states.

The phase space for a system of N particles is $6N$ dimensional where $3N$ of the coordinates corresponds to the different particles generalized positions labeled q_α. The remaining $3N$ degrees of freedom correspond to the different canonical momenta labeled p_α. One can introduce Γ as the set $\{q_1, \dots, q_{3N}, p_1, \dots, p_{3N}\}$ as a specific point in phase space with corresponding volume element $d\Gamma$. A complete description of the dynamical state of a system constitutes then a point Γ. If the system behaves classically[6] and a governing Hamiltonian is known, in principal the dynamical evolution can be calculated by integrating the canonical equations [19]

$$\begin{aligned} q_\alpha(t) &= \frac{\partial H}{\partial p_\alpha} \\ p_\alpha(t) &= -\frac{\partial H}{\partial q_\alpha} \end{aligned} \tag{2.51}$$

given initial conditions at time t_0. This constitutes $6N$ equations and is an impossible task since N is large, typically at the order of 10^{23} or more for macroscopic systems. In principle though, if the equations were solved the solution would map out a path through the phase space. This can be used to define the notion of a distribution function over the phase space in two different ways.

If a system is observed for a long time τ and the time spent in the neighborhood of a certain point in phase space is denoted as Δt (see Fig. 2.6 (a)), then the limit

$$\rho_N(\Gamma, t)d\Gamma = \lim_{\tau\to\infty} \frac{\Delta t(\Gamma, t)}{\tau} \tag{2.52}$$

defines a N particle probability density $\rho_N(\Gamma)$ corresponding to the uniform probability of finding the system of N particles in a specific state Γ at some time t. Alternatively, one can introduce a large collection constituting independent copies of the system randomly distributed over the phase space. Such a collection is called an ensemble (Fig. 2.6 (b)). One can define the probability density as the ratio between the number of points within the neighborhood of a point Γ and the total number of points.

In Appendix B the *Liouville equation* that governs the evolution of ρ is derived. With the use of the Poisson bracket[7] it is written as

$$\frac{d\rho_N}{dt} = \frac{\partial \rho_N}{\partial t} + \{\rho_N, H\} = 0. \tag{2.54}$$

6Classical in the sense that the system is well described by Newtonian mechanics.

7The Poisson bracket on quantity A is defined as

$$\{A, H\} = \sum_{i=1}^{3N} \left(\frac{\partial A}{\partial q_i}\frac{\partial H}{\partial p_i} - \frac{\partial A}{\partial p_i}\frac{\partial H}{\partial q_i} \right) \tag{2.53}$$

Solving the Liouville equation exactly is an impossible task, but there is some important knowledge gained by its introduction. Due to the conformity to the canonical equations the behavior of the distribution function is that of an incompressible fluid. This has the important implication that a volume element in phase space is invariant in time, a result known as *Liouville's theorem*. The main issue with ρ_N is that it contains to much information. Integrating over all but one of the subspaces, using $d\Gamma_1 = dq_1 dp_1$, produces a new density

$$\rho_1(\boldsymbol{q}, \boldsymbol{p}, t) = V \int \frac{d\Gamma}{d\Gamma_1} \rho_N(\Gamma) \tag{2.55}$$

called the *one particle density* representing a single particle in the averaged environment of all other particles in the system. The volume V of the system is needed so that the probability of finding the particle in a neighborhood of the six dimensional point $(\boldsymbol{q}, \boldsymbol{p})$ is

$$\frac{\rho_1(\boldsymbol{q}, \boldsymbol{p})}{V} d\Gamma_1. \tag{2.56}$$

Integrating Liouville's equation over $d\Gamma/d\Gamma_1$ results in

$$\frac{\partial \rho_1}{\partial t} + \{\rho_1, H\} - \left(\frac{\partial \rho_1}{\partial t}\right)\Big|_{scattering} = 0, \tag{2.57}$$

where the remaining parts of higher order densities have been collected in the last term, subscripted by scattering since this term contains the interaction between the isolated particle and all other particles. Using the canonical equations this may be reformulated in vector form

$$\frac{\partial \rho_1}{\partial t} = - \underbrace{\boldsymbol{v}}_{= \frac{\partial \boldsymbol{q}}{\partial t}} \cdot \nabla \rho_1 - \underbrace{\boldsymbol{F}_{ext.}}_{= \frac{\partial \boldsymbol{p}}{\partial t}} \cdot \nabla_{\boldsymbol{p}} \rho_1 + \left(\frac{\partial \rho_1}{\partial t}\right)\Big|_{scattering}. \tag{2.58}$$

The first term on the right hand side can be identified with a diffusive process and the second one as influenced by external forces so the equation can be written as

$$\frac{\partial \rho}{\partial t} = \left(\frac{\partial \rho}{\partial t}\right)\Big|_{diffusion} + \left(\frac{\partial \rho}{\partial t}\right)\Big|_{external\ fields} + \left(\frac{\partial \rho}{\partial t}\right)\Big|_{scatt.}. \tag{2.59}$$

This is the *Boltzmann equation* in its general form for a classical distribution of distinguishable particles. It states that the change in the one particle distribution is due to a balance between diffusion, external influence from e.g., electromagnetic or gravitational fields and internal scattering. It is an elegant compact description of the complex situation where external fields accelerate the particles feeding

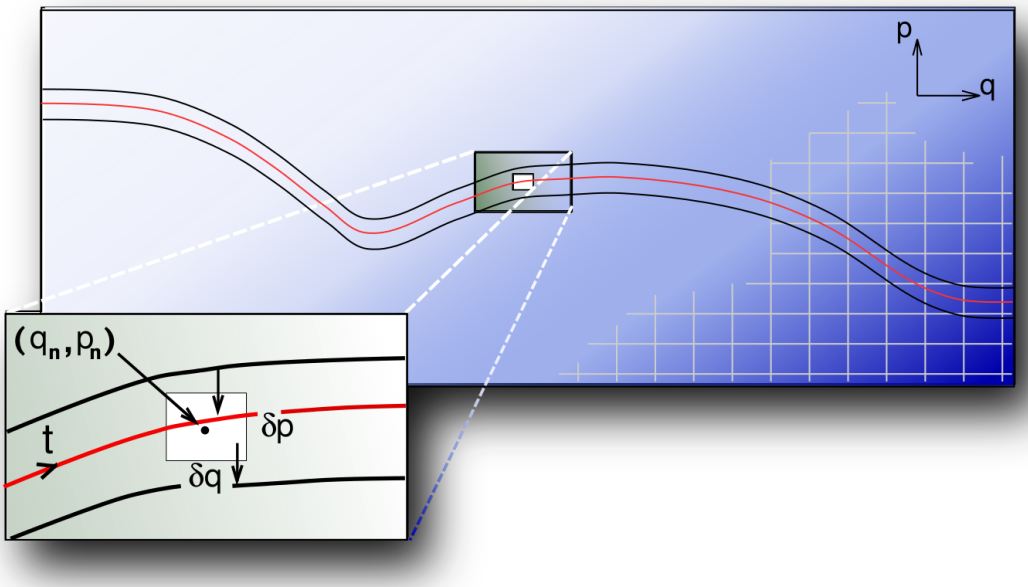

Figure 2.7: Due to scattering processes different paths in phase space may exchange states. Here it is schematically shown how states of certain momenta are scattered into the neighborhood of the path from the top path while states of certain momenta are scattered out of the neighborhood to the bottom path.

energy into the system shifting the occupation function while scattering events redistribute the energy dissipating it into the structure and relax the perturbed occupation function.

There is an alternative way to derive the Boltzmann equation via Liouville's theorem, that includes some physical intuition. To this end, one starts with neglecting scattering, which is reasonable for a sufficiently diluted system. Then one introduces a distribution $f(\boldsymbol{r}, \boldsymbol{p}, t)$ in the form of an occupation function that counts the number of states at $\boldsymbol{r}$ that have momenta $\boldsymbol{p}$ at time t. Because of Liouville's theorem the number of states in a neighborhood of the point at $(\boldsymbol{r}, \boldsymbol{p})$ at time t must all have been transported from another point in accordance with Newton's equations

$$\begin{aligned} \mathrm{d}\boldsymbol{r} &= \boldsymbol{v}\mathrm{d}t \\ \mathrm{d}\boldsymbol{p} &= \boldsymbol{F}\mathrm{d}t. \end{aligned} \tag{2.60}$$

Within the neighborhood, using a Taylor expansion the following holds true to first order in dt

$$\begin{aligned} f(\boldsymbol{r},\boldsymbol{p},t) &= f(\boldsymbol{r}-\boldsymbol{v}\mathrm{d}t,\boldsymbol{p}-\boldsymbol{F}\mathrm{d}t,t-\mathrm{d}t) \\ &= f(\boldsymbol{r},\boldsymbol{p},t)+\left.\frac{\partial f}{\partial r_\alpha}\right|_{(\boldsymbol{r},\boldsymbol{p},t)} v_\alpha \mathrm{d}t+\left.\frac{\partial f}{\partial p_\alpha}\right|_{(\boldsymbol{r},\boldsymbol{p},t)} F_\alpha \mathrm{d}t+\left.\frac{\partial f}{\partial t}\right|_{(\boldsymbol{r},\boldsymbol{p},t)} \mathrm{d}t \end{aligned} \tag{2.61}$$

where the Einstein sum convention applies. Canceling $f(\boldsymbol{r},\boldsymbol{p},t)$, identifying the total derivative and writing the equation in vector notation gives

$$\frac{df}{dt}=\frac{\partial f}{\partial t}+\boldsymbol{v}\cdot\nabla f+\boldsymbol{F}\cdot\nabla_{\boldsymbol{p}} f=0 \tag{2.62}$$

which must hold in each point of phase-space. Increasing the concentration the particles start to scatter. This means that particles with a certain momentum may be scattered in to a neighboring point in phase space. Alternatively, particles with a certain momentum can scatter out from a neighborhood (Fig. 2.7). This may be expressed symbolically by introducing a transition probability operator $P_{\boldsymbol{p}'\to\boldsymbol{p}}(\boldsymbol{r},\boldsymbol{p})$ giving the rate for states into the phase space point $(\boldsymbol{r},\boldsymbol{p})$. Similarly $P_{\boldsymbol{p}\to\boldsymbol{p}'}$ is the operator that expresses the rate of the states going out from $(\boldsymbol{r},\boldsymbol{p})$ as a result of scattering. Under normal circumstances it is reasonable to assume the principle of detailed balance, which means that in equilibrium the number of states scattered into a phase space point is balanced by an equal amount of states scattered out of the point. The effect of scattering vanishes and so the scattering term disappears. This suggests that the scattering term should appear as the difference of the two transition rates as

$$\boldsymbol{S}=P_{\boldsymbol{p}'\to\boldsymbol{p}}-P_{\boldsymbol{p}\to\boldsymbol{p}'}. \tag{2.63}$$

The rate of states transitioning into and out from the phase space point due to scattering must balance the total change of the occupation function. Including this effect of scattering in Eq. (2.64) the Boltzmann equation becomes

$$\frac{df}{dt}=\frac{\partial f}{\partial t}+\boldsymbol{v}\cdot\nabla f+\boldsymbol{F}\cdot\nabla_{\boldsymbol{p}} f=\boldsymbol{S}f. \tag{2.64}$$

2.4.1 The semiclassical assumption

The Boltzmann equation Eq. (2.64) may be rewritten using the quantum mechanical expression for the crystal momentum $\boldsymbol{p}=\hbar\boldsymbol{k}$

$$\frac{df}{dt}=\frac{\partial f}{\partial t}+\boldsymbol{v}\cdot\nabla f+\frac{\boldsymbol{F}}{\hbar}\cdot\nabla_{\boldsymbol{k}} f=\left(\frac{\partial f}{\partial t}\right)\Bigg|_{scattering}. \tag{2.65}$$

The appearance of $\hbar$ indicates that the equation may be applied in a quantum mechanical setting under certain conditions.

The distribution function needs to take into account that particles are indistinguishable. This is accomplished by letting the equilibrium distribution function describe either bosonic or fermionic statistics. In practice this means that the equilibrium distribution is either the Bose-Einstein or the Fermi-Dirac distribution.

In the quantum mechanical description the particles are described by wavefunctions. This has the implication that the velocity appearing in Eq. (2.65) is identified with the group velocity of the waves associated with the states in f. Particle position and momentum then cannot be determined simultaneously with arbitrary precision. Being conjugate operators with a non-vanishing commutator the uncertainty principle limits the precision to

$$\Delta x \Delta p \geq \hbar. \tag{2.66}$$

This is fine as long as Δx can be taken large enough to ensure low uncertainty in p. Since $\hbar$ is of the order 10^{-34} Js a granular view of x may be sufficient and still produce enough precision for the Boltzmann equation. The granularity is sufficient as long as the spatial extent of the wave packet is on a scale less than the mean free path between particle collisions.

According to the *Ehrenfest Theorem* the center of a wavepacket follows the path of a classical particle in a potential [20]. If the wavepacket is sufficiently localized on the scale of the potential the particle may, to a good approximation, be viewed as a classical particle in that potential. This has the implication that the potential must be slowly varying on the length scale of the wave packet. For time varying fields this also sets a temporal constraint so that the frequency associated with the time variation of the field may not become to large.

This is the basis for the semiclassical assumption and restricts the application of the Boltzmann equation to situations, in which quantum interference is not expected.

2.4.2 The relaxation time approximation

The scattering term in Eq. (2.64) is in general a complicated operator. Assuming that there are no external fields and that the system is spatially homogeneous the Boltzmann equation reads

$$\frac{\partial f}{\partial t} = \boldsymbol{S} f. \tag{2.67}$$

If we assume that the system is close to equilibrium the distribution function should be the equilibrium distribution f_0 with an added small perturbation formally writ-

ten as

$$\delta f = f - f_0. \tag{2.68}$$

If the internal scattering is assumed to relax the system, the simplest way to model this is to assume that the rate of change in the distribution function is reduced by the magnitude of the perturbation to the state, over a time scale τ. Equation 2.67 then becomes

$$\frac{\partial f}{\partial t} = \frac{\partial(\delta f)}{\partial t} = -\frac{\delta f}{\tau}. \tag{2.69}$$

with the solution

$$\delta f = \delta f(0) e^{-t/\tau} \tag{2.70}$$

indicating exponential decay of the perturbations over a characteristic time τ. It is natural to call this the relaxation time and the inclusion of the scattering term as in Eq. (2.70) for the *relaxation time approximation* (RTA).

2.4.3 Boltzmann transport for electrons in an electric field

As an example of a solution to the Boltzmann equation within the RTA the case of electrons in a static electric field is presented in this section. The next section considers the Boltzmann equation for phonons in a thermal gradient.

Electrons are fermions and as such obey *Fermi-Dirac* statistics. This is a result of the *Pauli exclusion principle*, which states that two fermions can not simultaneously be in the same quantum state. The occupation in thermal equilibrium at temperature T is then described by the Fermi-Dirac distribution

$$f_0 = \frac{1}{\exp\left(\frac{\varepsilon-\mu}{k_B T}\right) + 1}, \tag{2.71}$$

where ε is the energy of an electron with wave vector $\boldsymbol{k}$ and μ is the chemical potential of the electrons.

If a static electric field $\boldsymbol{E}$ is applied to the material the electrons will experience a Coulomb force accelerating them in the direction opposite to the the electric field. If the fundamental charge is q then the force on the electrons will be $\boldsymbol{F} = -q\boldsymbol{E}$. The electron energy and the chemical potential will then become spatially dependent. Assuming that the RTA holds in the steady state the Boltzmann transport equation is stated as

$$\frac{df}{dt} = \underbrace{\frac{\partial f}{\partial t}}_{=0} + \boldsymbol{v} \cdot \nabla f - \frac{q\boldsymbol{E}}{\hbar} \cdot \nabla_{\boldsymbol{k}} f = -\frac{\delta f}{\tau}. \tag{2.72}$$

If the perturbations are small compared to f_0 the variation in δf will be negligible compared to variations in f. The gradients of δf may then be dropped and the equation becomes

$$\boldsymbol{v} \cdot \nabla f_0 - \frac{q\boldsymbol{E}}{\hbar} \cdot \nabla_{\boldsymbol{k}} f_0 = -\frac{\delta f}{\tau}. \tag{2.73}$$

The perturbations may then be solved for algebraically as

$$\delta f = -\tau \left(\boldsymbol{v} \cdot \nabla f_0 - \frac{q\boldsymbol{E}}{\hbar} \cdot \nabla_{\boldsymbol{k}} f_0 \right). \tag{2.74}$$

Since the equilibrium distribution is known, this presents a full solution within the RTA up to the free parameters in the form of the relaxation times τ. These parameters must be measured, estimated or calculated from first principles.

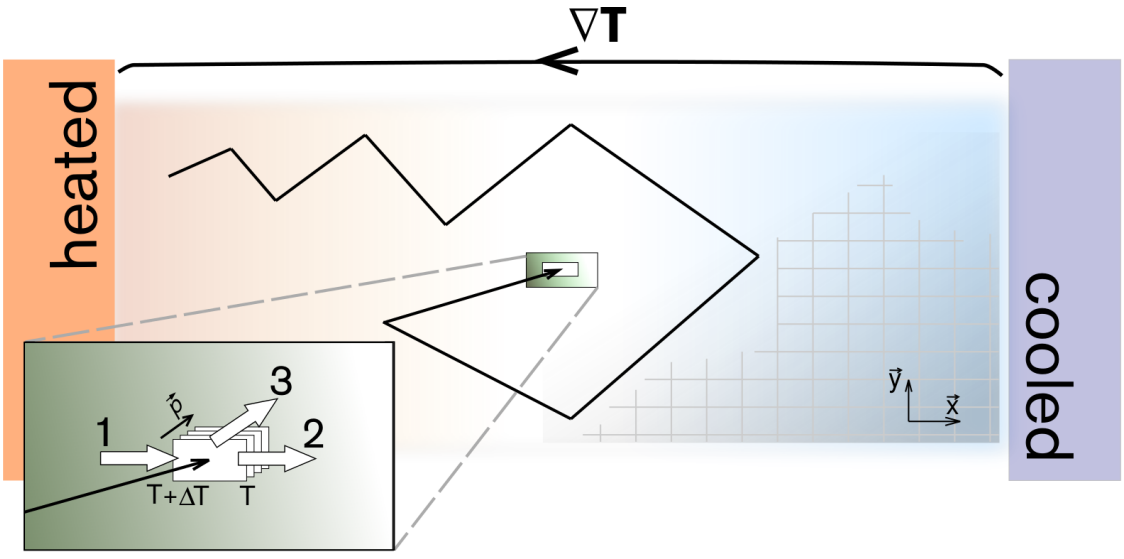

Figure 2.8: A particle experiencing several scattering events here shown in position space.

2.4.4 Boltzmann transport for phonons

In a crystal in thermal equilibrium at temperature T the phonon modes are distributed according to the Bose-Einstein distribution [18]

$$n_{0,\lambda} = \frac{1}{\exp\left(\hbar\omega_\lambda / k_B T\right) - 1}. \tag{2.75}$$

The distribution function counts the number of phonon modes in state λ. Here $\lambda = (\boldsymbol{q}, p)$ is a collective index for a phonon mode with wave-vector $\boldsymbol{q}$ and band index p. The energy carried by a single phonon mode λ is

$$E_\lambda = \frac{\hbar\omega_\lambda}{\exp\left(\hbar\omega_\lambda / k_B T\right) - 1}. \tag{2.76}$$

The specific heat c_λ associated with phonon mode λ is then

$$c_\lambda = \frac{\partial E_\lambda}{\partial T} = k_B \left(\frac{\hbar\omega_\lambda}{k_B T}\right)^2 n_{0,\lambda}(n_{0,\lambda} + 1). \tag{2.77}$$

When there is a thermal gradient present the temperature becomes position dependent. The phonons in question are assumed not to interact with the electromagnetic field and so the force related term drops out. Then in the steady state only the diffusive term from the total derivative survives

$$\frac{dn_\lambda}{dt} = \underbrace{\frac{\partial n_\lambda}{\partial t}}_{=0} + \boldsymbol{v}_\lambda \cdot \nabla n_\lambda + \underbrace{\boldsymbol{F}\frac{\partial n_\lambda}{\partial p}}_{=0} = \left(\boldsymbol{v}_\lambda \cdot \nabla T(\boldsymbol{r})\right)\frac{\partial n_{0,\lambda}}{\partial T}. \tag{2.78}$$

where in the second step the diffusive term has been linearized. Introducing the scattering operator $\boldsymbol{S}$ acting on the distribution the linearized phonon Boltzmann equation in its *canonical form* reads

$$-\left(\boldsymbol{v}_\lambda \cdot \nabla T(\boldsymbol{r})\right)\frac{\partial n_{0,\lambda}}{\partial T} + \boldsymbol{S} n_\lambda = 0 \tag{2.79}$$

emphasizing the balance between diffusion and scattering in a specific mode. So there is thus a balance between a diffusive process and scattering. Introducing the RTA the scattering term is

$$\boldsymbol{S} n_\lambda = -\frac{n_\lambda - n_{0,\lambda}}{\tau_\lambda} = -\frac{\delta n_\lambda}{\tau_\lambda}. \tag{2.80}$$

and solving for the perturbation gives the solution

$$\delta n_\lambda = -\tau_\lambda\left(\boldsymbol{v}_\lambda \cdot \nabla T(\boldsymbol{r})\right)\frac{\partial n_{0,\lambda}}{\partial T} = -\tau_\lambda\left(\boldsymbol{v}_\lambda \cdot \nabla T(\boldsymbol{r})\right)\frac{\hbar\omega_\lambda}{k_B T^2} n_{0,\lambda}(n_{0,\lambda} + 1). \tag{2.81}$$

for a specific phonon mode λ.

2.4.5 Lattice thermal conductivity within the RTA

The microscopic thermal energy current $\boldsymbol{J}_Q$ resulting from phonon transport is the sum of the occupation weighted energy flux of individual phonon modes. The heat flux in the Cartesian direction α is

$$J_{Q,\alpha} = \frac{1}{V}\sum_{\lambda} \hbar\omega_\lambda n_\lambda \boldsymbol{v}_{\lambda,\alpha} = \frac{1}{V}\sum_{\lambda} \hbar\omega_\lambda \delta n_\lambda \boldsymbol{v}_{\lambda,\alpha}. \tag{2.82}$$

Here V is the volume of the system under consideration, ω_λ is the frequency, n_λ is the occupation and $\boldsymbol{v}_\lambda = \nabla_{\boldsymbol{q}}\omega_\lambda$ the group velocity. In the second step the distribution has been replaced with the perturbation. This is because of time reversal symmetry. In equilibrium there will be no energy current since each phonon mode will have an associated mode with an equally energetic phonon in the opposite direction. The terms in Eq. (2.82) cancels in pairs.

Inserting the solution (2.81) in Eq. (2.82) gives an expression for the heat current

$$\begin{aligned} J_{Q,\alpha} &= -\frac{1}{V}\sum_{\lambda} \tau_\lambda \left(v_{\lambda,\beta}\partial_\beta T\right) \underbrace{k_B\left(\frac{\hbar\omega_\lambda}{k_B T}\right)^2 n_{0,\lambda}\left(n_{0,\lambda}+1\right)}_{=\, c_\lambda} \\ &= -\Big(\underbrace{\frac{1}{V}\sum_{\lambda} \tau_\lambda v_{\lambda,\alpha} v_{\lambda,\beta} c_\lambda)}_{=\, \kappa_{\alpha,\beta}(T)} \Big)\partial_\beta T \\ &= -\kappa_{\alpha,\beta}(T)\partial_\beta T \end{aligned} \tag{2.83}$$

where repeated Cartesian index β is implicitly summed. The introduced quantity $\kappa_{\alpha,\beta}$ can be identified through Fourier's law

$$\boldsymbol{J}_Q = -\kappa \cdot \nabla T \tag{2.84}$$

as the thermal conductivity tensor. The expression for the lattice thermal conductivty has one flaw. It contains free parameters in the τ_λ.

2.4.6 Determination of lifetimes

2.4.6.1 The perturbed lattice Hamiltonian

If a unit cell has the position vector $\boldsymbol{l}$ and an atom in that cell has the relative position $\boldsymbol{b}$ the position of the atom may be denoted $\boldsymbol{r}(\boldsymbol{lb})$, where $\boldsymbol{l}$ and $\boldsymbol{b}$ label the atom, and a displacement of this atom will then be

$$\boldsymbol{u}(\boldsymbol{lb}) = \boldsymbol{r}(\boldsymbol{lb}) - \boldsymbol{l} - \boldsymbol{b}. \tag{2.85}$$

For small displacements in a classical crystal the change in the potential energy can be expressed as a Taylor series in the displacements. Formally this is expressed as

$$\begin{aligned} U = U_0 &+ \sum_{\boldsymbol{lb}} \left.\frac{\partial U}{\partial u^\alpha(\boldsymbol{lb})}\right|_0 u_\alpha(\boldsymbol{lb}) \\ &+ \frac{1}{2}\sum_{\boldsymbol{lb}}\sum_{\boldsymbol{l'b'}} \left.\frac{\partial^2 U}{\partial u^\alpha(\boldsymbol{lb})\partial u^\beta(\boldsymbol{l'b'})}\right|_0 u_\alpha(\boldsymbol{lb})u_\beta(\boldsymbol{l'b'}) \\ &+ \frac{1}{6}\sum_{\boldsymbol{lb}}\sum_{\boldsymbol{l'b'}}\sum_{\boldsymbol{l''b''}} \left.\frac{\partial^3 U}{\partial u^\alpha(\boldsymbol{lb})\partial u^\beta(\boldsymbol{l'b'})\partial u^\gamma(\boldsymbol{l''b''})}\right|_0 u_\alpha(\boldsymbol{lb})u_\beta(\boldsymbol{l'b'})u_\gamma(\boldsymbol{l''b''}) + \dots . \end{aligned} \tag{2.86}$$

The repeated Greek indices, representing Cartesian directions, are implicitly summed over in pairs. The derivatives are taken at the equilibrium positions, hence the first order term vanishes by definition and the constant term is an arbitrary shift of the energy scale and is here chosen as the reference. Since force is the spatial derivative of the potential the first type of derivative can be rewritten as

$$\Phi_{\alpha\beta}(\boldsymbol{lb},\boldsymbol{l'b'}) = \left.\frac{\partial^2 U}{\partial u^\alpha(\boldsymbol{lb})\partial u^\beta(\boldsymbol{l'b'})}\right|_0 = -\left.\frac{\partial F_\beta(\boldsymbol{l'b'})}{\partial u^\alpha(\boldsymbol{lb})}\right|_0 \tag{2.87}$$

with the physical interpretation as the change in the force on the atom at $\boldsymbol{l'b'}$ as a response when atom $\boldsymbol{lb}$ is displaced. Similarly for the third order term

$$\Phi_{\alpha\beta\gamma}(\boldsymbol{lb},\boldsymbol{l'b'},\boldsymbol{l''b''}) = \left.\frac{\partial^3 U}{\partial u^\alpha(\boldsymbol{lb})\partial u^\beta(\boldsymbol{l'b'})\partial u^\gamma(\boldsymbol{l''b''})}\right|_0 = -\left.\frac{\partial^2 F_\gamma(\boldsymbol{l'b'})}{\partial u^\alpha(\boldsymbol{lb})\partial u^\beta(\boldsymbol{l'b'})}\right|_0 \tag{2.88}$$

relating the displacements of atoms to the force on atom $\boldsymbol{l''b''}$ when displacing atoms $\boldsymbol{lb}$ and $\boldsymbol{l'b'}$. These sets of constants are called the second and third order interatomic force constants (IFC). Up to third order the potential is expressed as

$$U = \frac{1}{2}\sum_{\boldsymbol{lb}} \Phi_{\alpha\beta}u_\alpha(\boldsymbol{lb})u_\beta(\boldsymbol{l'b'}) + \frac{1}{6}\sum_{\boldsymbol{lb}}\sum_{\boldsymbol{l'b'}} \Phi_{\alpha\beta\gamma}u_\alpha(\boldsymbol{lb})u_\beta(\boldsymbol{l'b'})u_\gamma(\boldsymbol{l''b''}). \tag{2.89}$$

Through quantization by introduction of creation and annihilation operators $a_{\boldsymbol{q},s}$ and $a^\dagger_{-\boldsymbol{q},s}$ the displacements may be promoted to operators expressed through the Fourier expansion

$$u_\alpha(\boldsymbol{lb}) = \frac{1}{\sqrt{N}}\sum_{\boldsymbol{lb}} \epsilon_{s,\alpha}(\boldsymbol{q})e^{-i\boldsymbol{q}\cdot\boldsymbol{r}(\boldsymbol{lb})}\sqrt{\frac{\hbar}{2m_{\boldsymbol{b}}\omega_s(\boldsymbol{q})}}\left(\hat{a}_{\boldsymbol{q},s} + \hat{a}^\dagger_{-\boldsymbol{q}s}\right), \tag{2.90}$$

where $\epsilon_{s,\alpha}(\boldsymbol{q})$ is the polarization of the mode and $m_{\boldsymbol{b}}$ the mass of the atom at position $\boldsymbol{b}$. Using this expansion the first sum in Eq. (2.89) together with the kinetic energy can be shown to give a Hamiltonian

$$H_0 = \sum_{\boldsymbol{q},s} \hbar\omega_s(\boldsymbol{q}) \left(\frac{1}{2} + \hat{a}^\dagger_{\boldsymbol{q},s} \hat{a}_{-\boldsymbol{q},s} \right) \tag{2.91}$$

that is the same as the sum of Hamiltonians for quantum harmonic oscillators. This Hamiltonian acts as an unperturbed state constituting a set of harmonic oscillators and the second series acts as a perturbation on that set. The Hamiltonian extended to the third order in the displacements may be written as

$$H^{(3)} = H_0 + H' \tag{2.92}$$

where

$$H' = \frac{1}{6} \sum_{\boldsymbol{lb}} \sum_{\boldsymbol{l'b'}} \sum_{\boldsymbol{l''b''}} \Phi_{\alpha\beta\gamma} u_\alpha(\boldsymbol{lb}) u_\beta(\boldsymbol{l'b'}) u_\gamma(\boldsymbol{l''b''}). \tag{2.93}$$

2.4.6.2 The physical picture

To understand the physical meaning of the perturbed Hamiltonian notice that there are three displacements containing the sum of a creation and an annihilation operator in the third order term in Eq. (2.89). Introducing a phonon field represented by a state-vector with the occupation of individual phonon modes

$$\phi = |n_{\boldsymbol{q}_1,s_1}, n_{\boldsymbol{q}_2,s_2}, \ldots\rangle, \tag{2.94}$$

where the excitations are harmonic oscillators. The creation and annihilation operators then work such that the annihilation operator lowers the phonon occupation $n_{\boldsymbol{q},s}$ by one phonon

$$\hat{a}_{\boldsymbol{q},s} | \ldots, n_{\boldsymbol{q},s}, \ldots\rangle \propto | \ldots, n_{\boldsymbol{q},s} - 1, \ldots\rangle, \tag{2.95}$$

and the creation operator raises the occupation by one phonon

$$\hat{a}^\dagger_{-\boldsymbol{q},s} | \ldots, n_{\boldsymbol{q},s}, \ldots\rangle \propto | \ldots, n_{\boldsymbol{q},s} + 1, \ldots\rangle. \tag{2.96}$$

Expanding the factors containing sums of creation and annihilation operators gives the following factors

$$\begin{aligned} &\left(\hat{a}_{\boldsymbol{q},s} + \hat{a}^\dagger_{-\boldsymbol{q},s} \right) \left(\hat{a}_{\boldsymbol{q}',s'} + \hat{a}^\dagger_{-\boldsymbol{q}',s'} \right) \left(\hat{a}_{\boldsymbol{q}'',s''} + \hat{a}^\dagger_{-\boldsymbol{q}'',s''} \right) = \\ &\quad \hat{a}_{\boldsymbol{q},s} \hat{a}_{\boldsymbol{q}',s'} \hat{a}_{\boldsymbol{q}'',s''} + \hat{a}_{\boldsymbol{q},s} \hat{a}_{\boldsymbol{q}',s'} \hat{a}^\dagger_{\boldsymbol{q}'',s''} + \hat{a}_{\boldsymbol{q},s} \hat{a}^\dagger_{\boldsymbol{q}',s'} \hat{a}_{\boldsymbol{q}'',s''} + \hat{a}_{\boldsymbol{q},s} \hat{a}^\dagger_{\boldsymbol{q}',s'} \hat{a}^\dagger_{\boldsymbol{q}'',s''} \\ &\quad + \hat{a}^\dagger_{\boldsymbol{q},s} \hat{a}_{\boldsymbol{q}',s'} \hat{a}_{\boldsymbol{q}'',s''} + \hat{a}^\dagger_{\boldsymbol{q},s} \hat{a}^\dagger_{\boldsymbol{q}',s'} \hat{a}_{\boldsymbol{q}'',s''} + \hat{a}^\dagger_{\boldsymbol{q},s} \hat{a}_{\boldsymbol{q}',s'} \hat{a}^\dagger_{\boldsymbol{q}'',s''} + \hat{a}^\dagger_{\boldsymbol{q},s} \hat{a}^\dagger_{\boldsymbol{q}',s'} \hat{a}^\dagger_{\boldsymbol{q}'',s''}. \end{aligned} \tag{2.97}$$

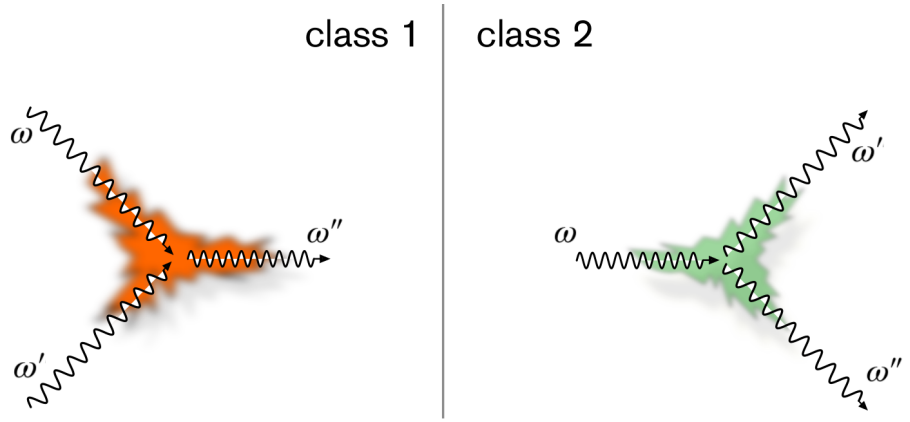

Figure 2.9: Schematic representation of class 1 and class 2 events. Class 1 events corresponds to the collision of two phonons with angular frequency ω and ω' annihilating into a phonon of angular frequency ω''. Class 2 events corresponds to the disintegration of a phonon mode of angular frequency ω annihilating into two phonons with angular frequency ω' and ω''.

Four different kinds of processes can be identified. One with three created phonons, one with three annihilated phonons, two created phonons annihilated into one phonon, and finally one created phonon annihilating into two phonons. The situation with only created or annihilated phonons are prohibited due to energy conservation and do not represent physical processes. Situations in which two phonons collide are called class 1 events and situations in which one phonon disintegrates into two new phonons are called class 2 events (Fig. 2.9). Energy conservation also applies to class 1 and 2 events. This can be expressed through factors of Dirac delta functions expressing energy conservation, $\delta(\omega + \omega' - \omega'')$ for class 1 events and $\delta(\omega - \omega' - \omega'')$ for class 2 events.

Besides energy conservation it is also necessary for the processes to respect the conservation of crystal momentum. A crystal in rest does not have any external momentum but the internal degrees of freedom are associated with a related quantity referred to as crystal momentum. But there is one difference, the crystal momentum must only be conserved up to a reciprocal lattice vector. This can be written as

$$\boldsymbol{q} + \boldsymbol{q}' = \boldsymbol{q}'' + \boldsymbol{G}, \tag{2.98}$$

for class 1 events and

$$\boldsymbol{q} + \boldsymbol{G} = \boldsymbol{q}' + \boldsymbol{q}'' \tag{2.99}$$

for class 2 events.

2.4.6.3 Lifetimes from first principles

It can be shown [21] that there is a relation between the imaginary part of the self energy Γ and the lifetimes through

$$\tau_\lambda = \frac{1}{2\Gamma_\lambda(\omega_\lambda)} \tag{2.100}$$

where Γ is

$$\Gamma_\lambda(\omega) = \frac{18\pi}{\hbar^2} \sum_{\lambda'\lambda''} |\Phi_{-\lambda\lambda'\lambda''}|^2 \Big\{ (n_{\lambda'} + n_{\lambda''} + 1)\ \delta(\omega - \omega_{\lambda'} - \omega_{\lambda''}) \\ + (n_{\lambda'} - n_{\lambda''}) \big(\delta(\omega + \omega_{\lambda'} - \omega_{\lambda''}) - \delta(\omega - \omega_{\lambda'} + \omega_{\lambda''}) \big) \Big\}. \tag{2.101}$$

The constants $\Phi_{-\lambda\lambda'\lambda''}$ are the Fourier transforms of the third order IFCs after a transformation to normal modes. This expression can be obtained with a version of Fermi's golden rule. The golden rule states that the rate from an in-state $|\phi_{in}\rangle$ to an out-state $|\phi_{out}\rangle$ due to a perturbation H' is obtained by evaluating

$$P_{in\to out} = \frac{2\pi}{\hbar} |\langle \phi_{out} | H' | \phi_{in} \rangle|^2 \delta(E_{out} - E_{in}). \tag{2.102}$$

The delta function assures that the energy is conserved in the process. Besides that, the Fourier transform of the IFCs contains a factor that is non-zero only in the case that the crystal momenta is conserved up to a reciprocal vector.

The problem then comes down to calculating the third order IFCs. In this thesis a direct approach has been taken. The constants can be directly calculated by using finite differences on force data obtained from an electron structure calculation (see Sect. 3.2). All the IFCs can be obtained by calculating the forces in structures obtained by displacing one atom for the second order IFCs, and two atoms for the third order IFCs [22, 23]. For efficiency the symmetry of the system should be used to single out an irreducible set of displacements needed for a complete description of the forces in the material.

2.5 Materials

2.5.1 van der Waals solids

The class of materials known as van der Waals solids consists of three-dimensional (3D) structures composed of monolayers of two-dimensional (2D) sheets, where the monolayers are bound together by interlayer van der Waals forces (Fig. 2.10). The sheets, in themselves, constitute a class called 2D materials, also known as single-layer materials. Here, 2D materials consist of a distinct monolayer, with a thickness corresponding to the atomic scale, and with an intralayer bonding of covalent, ionic, or possibly mixed covalent/ionic type.

Monolayers can be isolated from their 3D counterpart, by the use of a top-down approach where the weaker van der Waals bonds are broken without disrupting the in-plane integrity. The separation can, for instance, be done through micromechanical exfoliation using a scotch-tape technique, or exfoliation using liquid intercalation techniques. Alternatively, the monolayers can be synthesized in a bottom-up approach, using, for instance chemical vapor deposition (CVD) techniques [24]. The bottom-up approach allows for manufacturing of novel monolayers with a nonexistent 3D counterpart, for instance, silicene and germanene, the hexagonal monolayer allotropes of silicon and germanium.

With the improvement of manufacturing techniques for monolayers, either top-down or bottom-up, the family of isolated 2D materials has grown considerably in the last decade [25, 26, 24]. After the reported isolation of monolayers of graphite in 2004 [27], since then known as graphene, many other 2D materials have been isolated. Early, well-studied examples consist of hexagonal boron nitride (h-BN) and molybdenum disulfide (MoS_2) from the group of transition metal dichalcogenides (TMDs), a group associated with many different 2D materials. Today, there is a plethora of 2D materials besides the ones introduced. Examples include phosphorene, the monolayer of black phosphorous [28], and to phosphorene the isoelectronic group-IV monochalcogenides such as tin- and germanium selenides and sulfides (SnSe, SnS, GeSe, and GeS). Other interesting examples of monochalcogenides are the gallium and indium monochalcogenides. Worth mentioning, there are also groups of oxides with layered structures that are relevant for the research fields interested in 2D materials.

The electronic character of different 2D materials ranges from metals and semimetals, through semiconductors to dielectric insulators. The forerunners extensively examined within the 2D family, graphene, h-BN, and MoS_2 are individual examples of a 2D semimetal, insulator and semiconductor [29]. Besides graphene, the related silicene and germanene also form hexagonal semimetallic monolayers. The semimetallic character in these materials is related to a linear crossing in the bandstructure, at the Fermi-level, forming the so-called Dirac cones centered

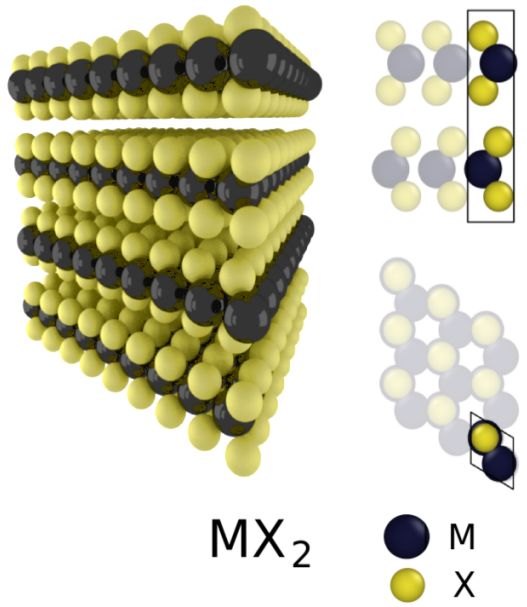

Figure 2.10: The crystal structure of the molybdenum and tungsten based transition metal dichalcogenides. The transition metal corresponds to M and the chalcogenide to X.

around the K and K' points. In the context of 2D materials, h-BN was originally used in its 3D form as an isolating substrate for graphene. Today, single layer h-BN is interesting for electronic applications or as a building block in heterostructures [30, 31, 32]. Among the TMDs, MoS_2 has a dominating position in research, in part because of the availability of molybdenite crystals used for exfoliation of mono- and few-layer MoS_2. The closely related semiconducting molybdenum and tungsten based dichalcogenides WS_2, $MoSe_2$ and WSe_2 have not been as extensively investigated although they have similar properties as MoS_2.

The properties of a 2D material can differ significantly from its corresponding 3D structure. The exotic band structure of graphene is one illuminating example. In the 3D allotrope graphite, the Dirac cones are not present. The significance of the linear dispersion in the band structure, is the implication of massless electron behavior and a constant universal electron velocity within the cones, in analogy with the universal speed limit associated with massless particles in special relativity [33]. Another illuminating example is the change of electronic properties in MoS_2 and WS_2 when comparing the electronic properties of the 3D bulk and corresponding 2D monolayers. The 3D bulk has an indirect bandgap of 1.2 eV and 1.3 eV respectively. In the corresponding monolayers, the band structure transforms in that the band gap increases and the bandstructure shifts into a direct band-

gap with values of 1.9 eV respectively 2.1 eV [34]. The nature of the bandgap is very fundamental in applications related to optoelectronic devices. When the bandgap is direct, the semiconductor can easily interact with photons of energies greater than the bandgap through emission and absorption processes. If the bandgap is indirect, an additional phonon has to be involved for the purpose of momentum conservation, rendering much less efficiency in the interaction with the photon field.

The emergence of new types of 2D materials paves the way for novel forms of van der Waals solids, known as van der Waals heterostructures [29]. In a van der Waals heterostructure, different types of monolayers are combined in a regular pattern, with the potential for dramatic changes in the material properties. The family of 2D materials, in themselves, cover a wide range of interesting properties. The concept of heterostructures introduces the promise of more control over these properties [35, 29, 25]. When stacked, the interaction between layers might induce changes in the charge distribution, as well as structural changes, in neighboring monolayers, which opens the possibility for managing these properties. Although the exciting prospect of heterostructures, there are still many obstacles to overcome in that the assembly techniques currently available are limited [25].

One group of van der Waals solids of interest, not only as primitive systems but also in the context of heterostructures, are the molybdenum and tungsten based TMDs. These TMDs has the general stoichiometry MX_2 where (M=Mo, W; X=S, Se, Te). The equilibrium structures are layered with hexagonal symmetry and an ABAB stacking of the planes (Fig. 2.10). The symmetry belongs to the space group $P6_3/mmc$ (International Tables of Crystallography No. 194), except for WTe_2 that has an orthorhombic symmetry in the space group $Pmn2_1$ (ITC No. 31).

Besides the interest in using molybdenum and tungsten based TMDs for electronic [36, 34] as well as optoelectronic applications [34, 37, 38], there is also potential for the use of these TMDs in spintronics [39]. Further, it has also been reported a significant increase in the thermoelectric figure of merit in MoS_2, based on first-principles calculations [40]. Although MoS_2, and related TMDs, have high Seebeck coefficients, the electrical conductivities are low [41, 42]. Yet, improvements might be made to the electron mobility through changes in the band structure by inducing stress in the systems[36]. In these applications is thermal transport important. Either for thermal management in electronic applications [43], or improvement of the thermoelectric efficiency. Thermal management is important for functionality, reliability and stability in electronic devices. And the thermoelectric efficiency can be improved by reduction of the thermal conductivity. It is therefore important to develop a detailed understanding of the thermal conductivity in TMDs.

As a result of the difference in the stronger intralayer bonding compared to out-of-plane van der Waals interaction, the thermal conductivity in the TMDs is highly

anisotropic. The out-of-plane thermal conductivity $\kappa_\perp$ is of the order of 1 W/mK at room temperature [44, 45, 46]. Interestingly, Chiritescu *et al.* reported a $\kappa_\perp$ of 0.05 W/mK in disordered thin films of WSe_2 [44], a reduction by a factor of 30 compared to single crystals. This value is remarkably low, even lower than the theoretical limit [47], and was attributed to randomization of the stacking order. In Paper I is the origin of this reduction investigated in more detail.

In general, the experimental values reported for the thermal conductivity in TMDs shows a considerable spread. In the case of the most investigated TMD, MoS_2, varies the reported value for the in-plane lattice thermal conductivity considerably, from 20 W/mK [48] to 100 W/mK [49]. The reason for this spread is probably related to the difficulties associated with experimental measurements in these type of structures, as well as sample size effects and sensitivity to defects. The different lattice thermal conductivities reported from calculations also show a significant variation. Most calculations are done with monolayers, possibly because the more common exchange-correlation functionals used in density functional theory have difficulties capturing the van der Waals interaction between the layers properly. Paper II investigates the thermal transport in bulk TMDs using Boltzmann transport theory. First-principles calculations with a van der Waals density functional is here used to accurately capture the interlayer interaction.

2.5.2 Inorganic clathrates

Clathrates, in general, are chemical substances with a well-defined lattice structure of an inclusion type [50, 51]. The structure constitutes a caged framework, also commonly referred to as the host structure, with the ability to trap atomic or molecular species, called the guest species. The name clathrate originates from the Latin word *clatratus* with the meaning "protected by a crossbar." One specific class of interest are the inorganic clathrates, e.g., $Ba_8Ga_{16}Ge_{30}$ and $Sr_8Ba_{16}Sn_{30}$, in that they have very favorable properties for thermoelectric performance. They have an intrinsic combination of low thermal conductivities, high Seebeck coefficients, and good dopability [52, 53]. $Ba_8Ga_{16}Ge_{30}$ is a well-studied clathrate and representative for other similar compounds. It has been well investigated both experimentally [54, 55, 56, 57, 58, 59], and theoretically [60, 61, 55, 62, 63], and is the clathrate investigated in Papers III and IV of this thesis.

The inorganic clathrates, also known as intermetallic clathrates, or Zintl clathrates [53], can in general be ordered into six different structure types, built from four different kinds of polyhedra. The most common type of inorganic clathrate, known as the type I clathrate (Fig. 2.11), is built from two of these polyhedra types, namely six larger tetrakaidekahedra, and two smaller pentagonal dodecahedra. The larger tetrakaidekahedra are joined by their hexagonal faces, forming

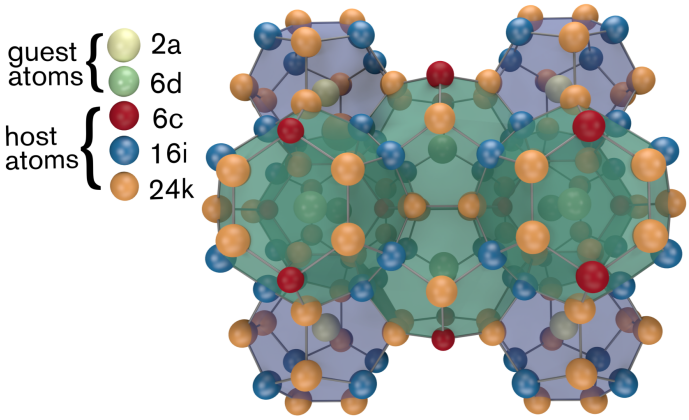

Figure 2.11: Crystal structure of type I clathrates. The guest species (Ba) occupies Wyckoff sites of type 2*a* and 6*d*, while the host species (Ga, Ge) occupy Wyckoff sites of type 6*c*, 16*i*, and 24*k*.

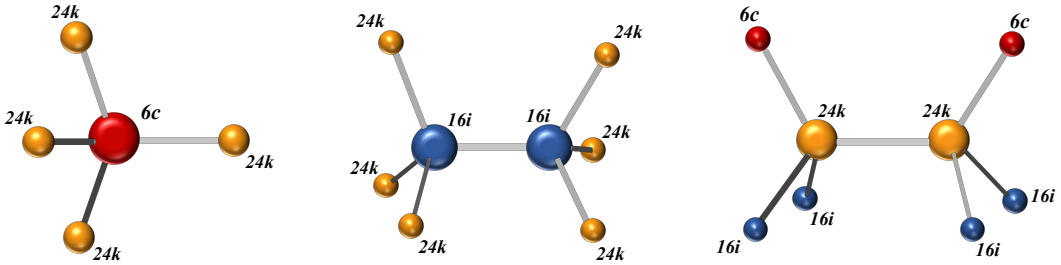

Figure 2.12: The relations between neighboring Wyckoff sites in the host structure of a type I clathrate. As seen from Wyckoff position 6*c* (left panel), position 16*i* (middle panel), and position 24*k* (right panel).

tubes stacked in the three orthogonal directions. The smaller dodecahedra are then fitted into the framework. Each polyhedron now contains a void in which a guest species can be trapped. The ideal type I clathrate structure belongs to space group $Pm\bar{3}n$ (international tables of crystallography number 223). The center of the cages in the structure offers eight sites for the guest species, in Wyckoff notation called sites 2*a* in the smaller cages, and sites 6*d* in the larger type of cage. The host system forms a framework of 46 tetrahedrally bonded atom positions, divided over three separate types of crystallographic sites, with Wyckoff symbols 6*c*, 16*i* and 24*k*, respectively.

A common ternary composition of semiconducting type I clathrates is $A_8B_{16}C_{30}$,

where A is an alkali earth metal or possibly a divalent rare earth metal, B an element from group 13, and C a group 14 element. The composition can be understood with the Zintl concept, i.e., the host structure is fully charge balanced. Assuming that the guest species donates two valence electrons to the host structure, the composition formula can be balanced for charge neutrality in the host, resulting in a composition ratio 16:30 for the host species [64]. It is common for real materials to deviate from this ratio. If there is a shift so that the amount of B increases, while the amount of C decreases, there is an excess of holes in the structure and the system becomes intrinsically p-doped. If the balance is shifted in the opposite direction, with an excess amount of C, there is an excess of electrons and the system becomes intrinsically n-doped.

The distribution of the elements in the host structure is not random but shows chemical ordering. If the positioning in the cage structure is fully randomized, one is expected to find species B occupying a specific site at approximately 35%, based on the 16:30 ratio. Experimental measurements of the site occupancy factors (SOFs) show that this is not the case [64]. For example, in $Ba_8Ga_{16}Ge_{30}$, the SOF for Ba at the 6*c* site varies between 60 to 75% in different samples. The SOF for the 16*i* site is shifted down to about 16-17%, while the 24*k* site SOF is between 30 and 40%. The reason for this deviation is the unfavorable energy cost for bonds between trivalent elements in the structure, this was established through calculations done by Blake *et al.* [61], and has been more recently investigated using alloy cluster expansions [65]. The unwillingness of sharing bonds with another trivalent element leads to a set of rules for the maximal SOFs for trivalent elements. As an example, the 6*c* site only connects to 24*k* sites (Fig. 2.12, left panel), and can in principle allow SOFs up to 100% for a trivalent element [64]. Both the 16*i* and 24*k* sites, on the other hand, share a bond with another similar site (Fig. 2.12, middle panel, and right panel), and should both be limited to SOFs of a maximum of 50%. The sum of the SOFs for site 16*i* and 24*k* should be less than 50% since the 16*i* site sees three 24*k* sites, and each 24*k* site sees two 16*i* site (Fig. 2.12, middle panel, and right panel). Then, according to this rule, it is not possible to randomly distribute trivalent elements on the 6*i* and 24*k* site.

The lattice thermal conductivities in type I inorganic clathrates are intrinsically very low, about 1 W/mK at room temperature. The low thermal conductivity can be attributed to the complexity of the primitive cell, and the presence of "rattling" guest species in the cages. An investigation of the phonon dispersion in, e.g., $Ba_8Ga_{16}Ge_{30}$ (Fig. 2.13, left panel) shows branches of a localized character, already at lower energies. Starting at approximately 2-3 meV there are numerous localized branches up to about 12 meV. Investigating the partial density of states reveals that it is the Ba guests associated with the 6*d* Wyckoff site that dominantly contributes to the localized branches at lower energies (Fig. 2.13, right panel). At somewhat higher energies, from 6-7 meV to 12 meV, the localized branches are

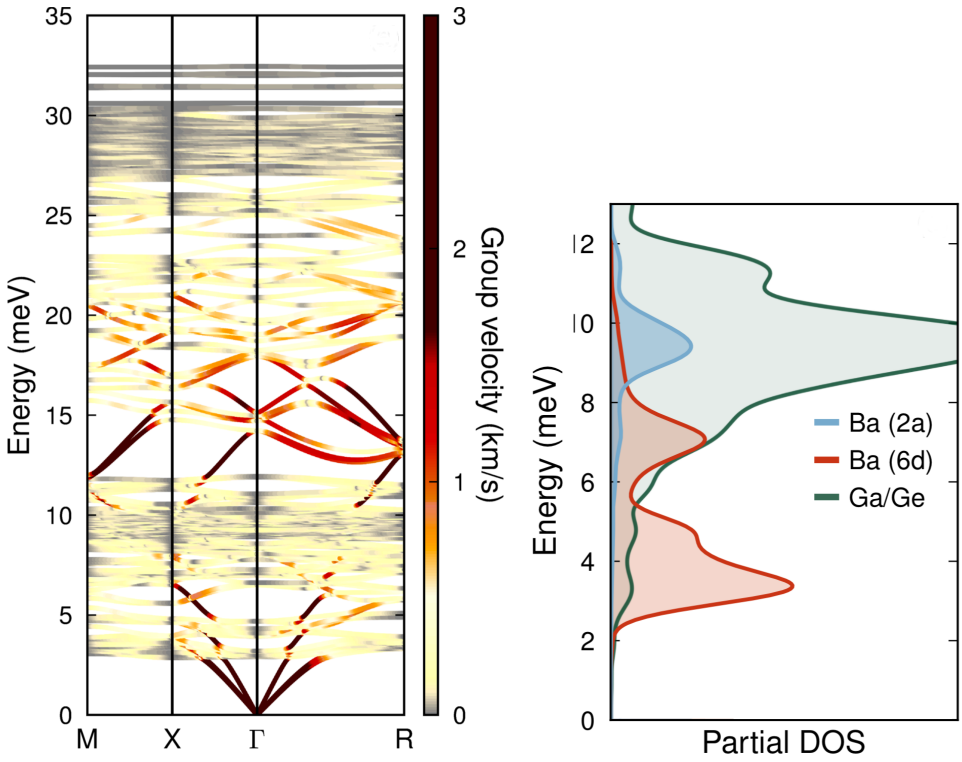

Figure 2.13: The left panel shows the phonon dispersion in $Ba_8Ga_{16}Ge_{30}$, color coded by the group velocity. The right panel shows the partial density of states in $Ba_8Ga_{16}Ge_{30}$, for Ba in the small cages at Wyckoff position 2*a* (blue line), Ba in the larger cage at Wykoff position 6*d* (red line), and the combined Ga/Ge cage (green line).

dominated by contributions from the Ga/Ge host structure.

In general, the trend for the lattice thermal conductivity κ_L in systems of increasing complexity is a reduction in κ_L [66]. A simple system, with a single atom in the primitive cell, can only have acoustic phonon modes. Each addition of an atom to the primitive cell introduces three new optical phonon modes. With increasing complexity, the additional number of optical phonon modes have a significant suppressing effect on the heat carrying acoustic modes, reducing κ_L. In the limit of an amorphous system, the acoustic contribution approaches zero, and the lattice mediated heat transfer is predominantly attributed to diffusion between atomic oscillators. The heat transport is then said to be glass-like.

With the inclusion of guest species, the heat capacity will increase, and κ_L might potentially become higher. On the other hand, if the guest atoms have highly anharmonic potentials, the increase in Umklapp scattering may instead introduce a decrease in κ_L. Further, if the guest species is under-constrained and weakly

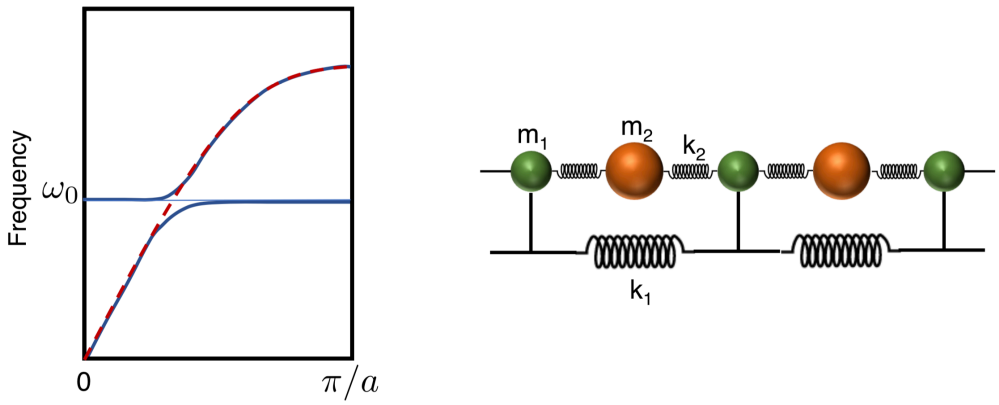

Figure 2.14: The left panel shows a schematic of an avoided band crossing at a resonance frequency ω_0, associated with the one-dimensional mass-spring system, shown in the right panel. The red dashed line correspond to the undisturbed acoustic mode in the absence of rattlers.

bound, the phenomena called rattling may occur. The effect of rattlers was at first thought to affect the phonon relaxation times through resonant scattering, resulting in a reduced κ_L [67]. An alternative mechanism is related to the group velocities. This mechanism can be understood by investigating a one-dimensional model (Fig. 2.14, right panel), analogous to the host/guest system of clathrates [68]. Assuming an alternating chain of masses m_1 coupled to masses m_2, with a coupling k_2. At the same time is the masses m_1 coupled to each other with a coupling k_1. A local resonance can occur when $k_2 \ll k_1$, with the possibility of the optical branch getting shifted to lower frequencies, resulting in an avoided band crossing, where the acoustic branch gets deflected (Fig. 2.14, left panel). The group velocity is then diminished at the resonance frequency resulting in a reduction of κ_L. The existence of rattler modes in clathrates has been theoretically predicted [63], showing good agreement with inelastic neutron scattering experiments. Rattling modes and avoided band crossings in clathrates have also been experimentally observed by Christensen *et al.* using triple axis spectroscopy on single crystal $Ba_8Ga_{16}Ge_{30}$ [68].

The overall effect on the lattice thermal conductivity, as the result of both complexity, and the presence of rattlers, has been theoretically investigated in the case of germanium-based type I clathrates by Dong *et al.* [69], using molecular dynamics with the Green-Kubo method. For pristine germanium in the diamond structure, they computed a lattice thermal conductivity of 114 W/mK at room temperature (the experimental value is 62 W/mK according to Ref. [70]). They further computed an estimate for the lattice thermal conductivity in an empty germanium cage Ge_{46}, resulting in a value of 12.2 W/mK, suggesting that the increased complexity in the caged structure gives an order of magnitude reduction for the conductivity.

Finally they introduced the effect of rattlers through the inclusion of Sr guests in the Ge_{46} framework, calculating a lattice thermal conductivity of 1.64 W/mK (the experimental value of $Sr_8Ga_{16}Ge_{30}$ is 0.89 W/mK [71]). Suggesting yet another order of magnitude reduction in the lattice thermal conductivity with the addition of rattlers. Compared to the thermal conductivity of 0.5 W/mK in amorphous Ge [47], this shows that the combined effect gives a structure with a thermal conductivity comparable to the thermal conductivity in glasses.

Because of the very low thermal conductivity and good performance as thermoelectric materials inorganic clathrates are thought of as a realization of the phonon glass-electron crystal concept [13], i.e., a system with the combination of low thermal conductivity and good electronic properties. The thermal conductivity in glasses typically has a T^2 dependence at really low temperatures [67]. In the following temperature range, the thermal conductivity levels out and plateaus. In the continuing range up to room temperature, the thermal conductivity slowly increases. In contrast, in materials with crystal-like thermal conductivity, the conductivity instead increases to a peak at lower temperatures, eventually followed by a $1/T$ decrease at higher temperatures. Both the crystal-like peak and the glass-like plateau have been reported for the lattice thermal conductivity in different inorganic clathrates [64].

3 Methods

3.1 Molecular dynamics simulations

The Boltzmann equation has some problems handling effects that deviate from bulk homogeneous effects, for instance interfaces. One alternative approach that can handle these difficulties is molecular dynamics (MD) [72].

MD is in general an entirely classical method where, assuming the atomic force fields are known, integration of Newtons equation for a collection of interacting atoms is performed. One illuminating example of the MD method is the use of Verlet integration [73] to Newtons equations. Given interatomic forces $\boldsymbol{F}$ acting on an atom, Newton's equation of motion for that atom are

$$\boldsymbol{F} = m\boldsymbol{a}, \tag{3.1}$$

where m is the mass of the atom and $\boldsymbol{a}$ its acceleration. To integrate Eq. (3.1) one approach is to Taylor expand the position $\boldsymbol{r}$ around some time t giving

$$\begin{aligned}\boldsymbol{r}(t+\Delta t) &= \boldsymbol{r}(t) + \boldsymbol{v}(t)\Delta t + \frac{1}{2}\boldsymbol{a}(t)\Delta t^2 + \frac{1}{6}\boldsymbol{j}(t)\Delta t^3 + \mathcal{O}(\Delta t^4),\\ \boldsymbol{r}(t-\Delta t) &= \boldsymbol{r}(t) - \boldsymbol{v}(t)\Delta t + \frac{1}{2}\boldsymbol{a}(t)\Delta t^2 - \frac{1}{6}\boldsymbol{j}(t)\Delta t^3 + \mathcal{O}(\Delta t^4),\end{aligned} \tag{3.2}$$

where $\boldsymbol{j}$ is the jerk. Addition gives the Verlet integration as

$$\boldsymbol{r}(t+\Delta t) = 2\boldsymbol{r}(t) - \boldsymbol{r}(t-\Delta t) + \boldsymbol{a}(t)\Delta t^2 + \mathcal{O}(\Delta t^4). \tag{3.3}$$

This integration scheme is accurate to fourth order in time, velocity independent and only requires knowledge of the positions in the current as well as the last time

step. Starting from two initial steps it is then possible to evolve the system in accordance with Newton's laws of motion.

Two limitations of MD can be mentioned. First, MD is a completely classical method and as such the average energy per phonon mode is $k_B T$ and can differ quite a bit from the true energy [74] see Eq. (2.76). Secondly, the number of atoms that need to be included can be quite high. To capture the behavior of a phonon the simulation domain should be at least twice as large as the respective phonon mean free path. Since the mean free path can be on the order of tens to hundreds of nanometers the number of atoms in the simulation may become intractable [74].

For MD simulations aiming at calculating the thermal conductivity there are two main approaches, the Green-Kubo method and the "direct method" [75] in the form of non-equilibrium molecular dynamics (NEMD).

The Green-Kubo method is an equilibrium approach where the equilibrium fluctuations are used to determine the lattice thermal conductivity through the Green-Kubo relations [76, 77, 78]. The Green-Kubo method exhibits slower convergence than than NEMD and thus requires more time steps [79]. It has also been demonstrated that there generally is an inconsistency between the results of the two methods in the case of conductance at the interface between two crystals [80].

The direct method, NEMD is much more straight forward. Typically, a simulation domain is set up with one hot region and cold region some distance apart. The outer regions are then connected through a periodic boundary. By fixing the temperature in the hot region a temperature gradient can be established between the hot and the cold region by the use of an appropriate thermostat or swapping method. When a steady state has established and if the simulation has been properly done, the thermal conductivity can be determined with the use of Fourier's law.

3.2 Atomic forces from first principles

The IFCs introduced in Sect. 2.4.6 are calculated from knowledge of the forces between interacting atoms. In the present thesis, these forces were computed using quantum mechanical calculations.

The wave function of a quantum mechanical system $|\Psi\rangle$ is governed by the *Schrödinger equation* [81, 82]

$$i\hbar \frac{\partial |\Psi(t)\rangle}{\partial t} = H |\Psi(t)\rangle , \tag{3.4}$$

where the Hamiltonian H describes both internal and external interactions. The eigenspace of H is given as the solution to the eigenvalue problem

$$H |\psi\rangle = E |\psi\rangle . \tag{3.5}$$

The eigenvalues E are by *definition* the possible energies in a quantum mechanical system and thus solving Eq. (3.5) has merits of its own. The vectors $|\psi\rangle$ form a suitable basis for expanding the system $|\Psi\rangle$ and are the building blocks if one wants to construct a solution to Eq. (3.4).

In general, solving the Schrödinger equation directly is an impossible task, just as solving the Liouville equation, Eq. (2.54). The reason being that the quantum mechanical state is multidimensional in nature. This is a result [83] of the indistinguishable nature of quantum particles and the probabilistic interpretation of quantum states in accordance with the Born rule [84].

In matter the Hamiltonian can generally be written [85]

$$\begin{aligned} H = &- \frac{\hbar}{2m_e} \sum_i \nabla_i^2 - \frac{\hbar}{2M_I} \sum_I \nabla_I^2 \\ &+ \frac{1}{2} \frac{1}{4\pi\epsilon_0} \sum_{i \neq j} \frac{e^2}{|\boldsymbol{r}_i - \boldsymbol{r}_j|} - \frac{1}{4\pi\epsilon_0} \sum_{i,I} \frac{Z_I e^2}{|\boldsymbol{r}_i - \boldsymbol{R}_I|} - \frac{1}{4\pi\epsilon_0} \sum_{I,J} \frac{Z_I Z_J e^2}{|\boldsymbol{R}_I - \boldsymbol{R}_J|}, \end{aligned} \tag{3.6}$$

where M_I and Z_I are the mass and charge of a nuclei, m_e the mass of an electron, e the fundamental charge and ϵ_0 the permittivity of free space. The position vectors $\boldsymbol{r}_i$ and $\boldsymbol{R}_I$ are with respect to an electron respectively a nuclei. The first two sums are operators for the kinetic energy of the electrons and the nuclei. The third sum comprises operators for the Coulomb interaction between electrons. The fourth sum contains interactions between electrons and the nuclei and the fifth, interactions between the nuclei.

The motion of the electrons and the nuclei are usually on such different timescale that the electronic part of the wave function can be separated from the part concerning the nuclei. Then the nuclei can be seen as frozen from the point of the electrons. This allows for a treatment where the electrons are viewed separately from the nuclei as an external potential, here noted V_{ext}. The Hamiltonian can now be written as[1]

$$h = -\frac{1}{2} \sum_i \nabla_i^2 + \frac{1}{2} \sum_{i \neq j} \frac{1}{|\boldsymbol{r}_i - \boldsymbol{r}_j|} + V_{ext}. \tag{3.7}$$

When the Schrödinger equation is solved for this system the force on the nuclei can be calculated with the Hellmann-Feynman force theorem [86]. With a solution for the ground-state energy E the theorem states that the force on ion I is given by

$$\boldsymbol{F}_I = -\frac{\partial E}{\partial \boldsymbol{R}_I}. \tag{3.8}$$

[1]From here on Hartree units will be used. Then action is then measured in units of the reduced Planck constant, charge in units of the fundamental charge and mass in units of electron masses. Finally the vacuum permittivity is set to $1/4\pi$.

Still there is a problem. The Hamiltonian in h generates a problem with many degrees of freedom albeit the great simplification from the Born-Oppenheimer approximation. Also because of the term describing electron interaction the wave function is not separable into one-electron wave functions. There is thus still a need for further simplifications of the electronic structure problem defined by h.

3.3 Density functional theory

Density functional theory (DFT) nowadays refers to a collection of first-principals techniques using the electron density as a fundamental variable. The electron density in a system of electrons is defined as the number density of electrons in a specific state [87]. Suppressing spin the electron density is derived from the many-body electron wave function $|\Psi\rangle$ as

$$\rho(\boldsymbol{r}_1) = N \int d\boldsymbol{r}_2 \dots \boldsymbol{r}_N \left|\Psi\right|^2. \tag{3.9}$$

If possible, the electron density is a much leaner object to work with, compared to the multidimensional wave function.

Fortunately, Hohenberg and Kohn showed in 1964 [88] that the electron density can be considered as a fundamental property of the ground state in that the ground state wave function can be expressed as a functional of the electron density $\rho_0(\boldsymbol{r})$. Hence the ground state energy may be expressed as

$$E_0 = \langle \Psi[\rho_0(\boldsymbol{r})] \big| h \big| \Psi[\rho_0(\boldsymbol{r})] \rangle. \tag{3.10}$$

They also showed that there exist a general functional $F[\rho]$ expressing the energy contribution from the kinetic energy as well as the interaction among the electrons. Together with a part giving the interaction energy from electronic interaction with the external potential V_{ext}, the energy can be expressed as

$$E[\rho(\boldsymbol{r})] = F[\rho(\boldsymbol{r})] + \int d\boldsymbol{r}\ \rho(\boldsymbol{r}) V_{ext}(\boldsymbol{r}). \tag{3.11}$$

This energy is minimized by the ground state density. Unfortunately the functional is not known in general. The theorem shows its existence but gives no prescription on how to find F. Since the functional contains many-body effects that are not known it is not possible to use this formulation, that is F directly [89].

3.3.1 The Kohn-Sham ansatz

In 1965 Kohn and Sham [90] proposed an ansatz where the system of interacting electrons is recast into a system of non-interacting electrons, a much simpler problem than the original many-body problem. The main assumption is that if one can

formulate an auxiliary problem, with the same ground state solution as in the full many-body problem, then a solution to the auxiliary system also solves the original problem. In the Kohn-Sham ansatz the functional $F[\rho(\boldsymbol{r})]$ in Eq. (3.11) is separated as

$$F[\rho(\boldsymbol{r})] = T_s[\rho(\boldsymbol{r})] + E_H[\rho(\boldsymbol{r})] + E_{xc}[\rho(\boldsymbol{r})]. \tag{3.12}$$

Here $T_s[\rho(\boldsymbol{r})]$ is the kinetic energy for non-interacting electrons and $E_H[\rho(\boldsymbol{r})]$ is the Hartee energy expressed as

$$E_H[\rho(\boldsymbol{r})] = \frac{1}{2}\int d\boldsymbol{r}d\boldsymbol{r}' \, \frac{\rho(\boldsymbol{r})\rho(\boldsymbol{r}')}{|\boldsymbol{r}-\boldsymbol{r}'|}. \tag{3.13}$$

Both of these terms are known. The unknown part $E_{xc}[\rho(\boldsymbol{r})]$ collects the more complicated many-body effects that are usually referred to as exchange and correlation.

In practice an effective potential is formulated as

$$V_{eff} = V_{ext} + V_H + V_{xc} \tag{3.14}$$

where V_H is the Hartree potential

$$V_H(\boldsymbol{r}) = \int d\boldsymbol{r}' \, \frac{\rho(\boldsymbol{r}')}{|\boldsymbol{r}-\boldsymbol{r}'|} \tag{3.15}$$

while the potential for exchange-correlation V_{xc} is the functional derivative of the exchange-correlation energy

$$V_{xc} = \frac{\delta E_{xc}[\rho(\boldsymbol{r})]}{\delta\rho(\boldsymbol{r})}. \tag{3.16}$$

The independence of the electrons allows for separation into single electron equations

$$\left(-\frac{1}{2}\nabla^2 + V_{eff}(\boldsymbol{r})\right)\psi_i(\boldsymbol{r}) = \varepsilon_i\psi_i(\boldsymbol{r}). \tag{3.17}$$

The Kohn-Sham orbitals $\psi_i(\boldsymbol{r})$ are under the constraint that

$$\rho(\boldsymbol{r}) = \sum_i f_i\left|\psi_i\right|^2, \tag{3.18}$$

where f_i is an occupation factor for electron state ψ_i. The formulation is exact although the functional for the exchange-correlation energy, $E_{xc}[\rho(\boldsymbol{r})]$ is unknown. Besides that there has been a great reduction in complexity from a quantum many-body problem into separate problems for independent electrons.

3.3.2 Exchange-correlation functionals

The unknown exchange-correlation functionals are in general complicated and approximations are necessary. The approximation presented in the original Kohn and Sham paper [90] assumes that the electron density in a local region is the same as the density in a uniform electron gas of density $\rho(\boldsymbol{r})$. The exchange-correlation energy is then given by

$$E_{xc}^{LDA}[\rho(\boldsymbol{r})] = \int d\boldsymbol{r}\ \rho(\boldsymbol{r})\varepsilon_{xc}^{LDA}[\rho(\boldsymbol{r})] \tag{3.19}$$

where the exchange-correlation energy for the uniform gas has a known solution [85]. The approximation is relatively simple considering the full problem, but has nonetheless proven itself in many applications over the years.

The LDA assumes a slowly varying electron density, so a natural step is to include effects of local variations in the exchange-correlation functional. This approach is the semi-local *generalized gradient approximation* (GGA). Here the exchange-correlation energy is assumed to be dependent on the electron density as well as the gradient of the density

$$E_{xc}^{GGA}[\rho(\boldsymbol{r}] = \int d\boldsymbol{r}\ \rho(\boldsymbol{r})\varepsilon_{xc}^{GGA}[\rho(\boldsymbol{r}), \nabla\rho(\boldsymbol{r})]. \tag{3.20}$$

There are many versions of GGAs. Most notable is the PBE functional [91], which has been successfully used in many applications.

3.3.3 van der Waals density functionals

The van der Waals force is the result of non-local correlation between electrons. Because of the non-local nature of the van der Waals force, it is not expected that a local or semi-local approximation will give a correct exchange-correlation energy.

In Papers I and II, first-principles calculations were conducted on van der Waals solids [35]. To describe van der Waals solids properly within DFT it is important to use a proper a van der Waals density functional (vdW-DF) that captures the sparse nature [92] of the materials. In 2003 a vdW-DF addressing layered structures [93] was presented, followed one year later by a vdW-DF for general structures [94].

In the vdW-DF method the correlation energy assumes a non-local form, which is expressed as a double integral over the spatial degrees of freedom [95]

$$E_c^{\mathrm{nl}}[\rho] = \frac{1}{2}\int\int \rho(\boldsymbol{r})\phi(\boldsymbol{r},\boldsymbol{r}')\rho(\boldsymbol{r}')d^3\boldsymbol{r}d^3\boldsymbol{r}', \tag{3.21}$$

where the kernel $\phi(\boldsymbol{r},\boldsymbol{r}')$ represents the non-local coupling of the electron densities at $\boldsymbol{r}$ and $\boldsymbol{r}'$. The correlation energy is usually complemented by a semi-local

exchange functional,

$$E_{xc}^{vdW-DF}[\rho(\boldsymbol{r})] = E_x^{sl}[\rho(\boldsymbol{r})] + E_c^{nl}[\rho(\boldsymbol{r})], \tag{3.22}$$

which historically was adapted from other semi-local exchange-correlation functionals. In 2014 a consistent exchange (CX) part was developed leading to the so-called vdW-DF-CX functional [96], which was used in Papers I and II of the present thesis.

3.3.4 Fourier expansion and pseudopotentials

In a solid, periodic boundary conditions are suitable for calculating bulk properties where surface effects are negligible. This is reasonable if the considered system is large compared to the boundaries. Effectively, by introducing periodic boundaries the computational system becomes infinite. In the case of a wave function, due to the theorem by Bloch [97] it is possible to expand the wave function in a plane wave basis set that is complete as long as the wave vectors in the first Brillouin zone are included. This is done by Fourier expansion over the reciprocal lattice vectors $\boldsymbol{G}$ through the series

$$\psi_{n,\boldsymbol{k}}(\boldsymbol{r}) = \sum_{\boldsymbol{G}} c_{n,\boldsymbol{k}+\boldsymbol{G}} \exp\left[i(\boldsymbol{k}+\boldsymbol{G})\cdot\boldsymbol{r}\right]. \tag{3.23}$$

This sum is infinite and for practical purposes the series must be truncated by a cutoff. The Fourier coefficients $c_{n,\boldsymbol{k}+\boldsymbol{G}}$ decrease for increasing $\left|\boldsymbol{k}+\boldsymbol{G}\right|$ [89]. So introduction of an energy cutoff E_{cut} allows for expansion including only the reciprocal vectors that fulfill the condition

$$\frac{\hbar^2}{2m}\left|\boldsymbol{k}+\boldsymbol{G}\right|^2 < E_{cut}. \tag{3.24}$$

With an increasing number of nodes, a wave function picks up an oscillating behavior near the nuclei [98]. Oscillations are more complicated to handle computationally and cause slow convergence[2]. Since core electrons are not strongly involved in interaction with valence electrons, for the sake of chemical bonding, it is not necessary to have a detailed description of the wave functions close to the nuclei. To overcome this issue one frequently employs so-called pseudopotentials, which replace the full Coulomb potential corresponding to the ionic core with a smoother potential that incorporates the core electrons and has the same scattering properties as the original potential [85]. Common schemes include norm-conserving and ultra-soft pseudopotentials [99]. In the present work the project augmented wave (PAW) [100] method was employed, which represents a bridge between pseudopotential and all-electron type calculations.

[2]More coefficients are necessary in the Fourier expansion

4

Summary of the papers

4.1 Paper I: Ultra-low thermal conductivity in WSe_2

Tungsten diselenide (WSe_2) is a van der Waals (vdW) solid that consists of two-dimensional sheets with strong intralayer bonding and interplanar vdW coupling. Van der Waals solids have a highly anisotropic thermal conductivity with an out-of-plane conductivity $\kappa_\perp$ for bulk material of 1.5 W/mK at room temperature [44]. It was experimentally demonstrated that $\kappa_\perp$ in turbostratically deposited WSe_2 films can be reduced down to 0.05 W/mK. This is a factor of 30 lower than in bulk crystals and thus considerably below the conservative estimate of the minimum thermal conductivity thought achievable.

In this paper a microscopic model was developed to explain this observation of an ultra-low thermal conductivity in disordered thin films of WSe_2. This was accomplished within the framework of Boltzmann transport theory and the relaxation time approximation (Sect. 2.4.5) based on second order force constants calculated within density functional theory. To accurately capture nonlocal correlation effects a non-empirical consistent exchange vdW density functional (vdW-DF-cx) was used [96].

First the sensitivity of the lattice thermal conductivity to different planar defects was established. Stacking disorder and strain cause phonon localization and softening of the acoustic modes, which can account for a reduction of $\kappa_\perp$ by a factor of 2 to 4 (green dashed line in Fig. 4.1). In addition the layer disorder introduces a structural limit on the phonon mean free path, which can be reduced to the separation between individual layers. Assuming that this limitation can be modeled by a diffuse boundary scattering model reduces the conductivity as well (green band

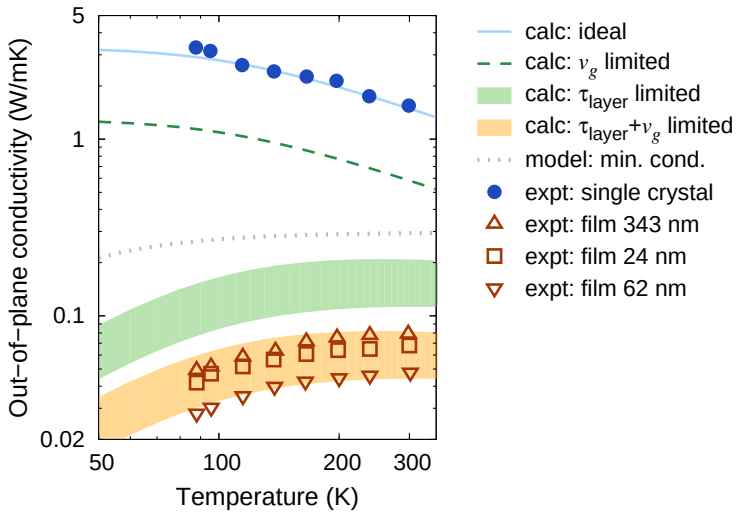

Figure 4.1: The experimentally measured reduced lattice thermal conductivity in disordered thin WSe_2 films corresponds to the red triangles and squares (Cahill et. al. [44]). The measured values in a single bulk crystal corresponds to the blue dots. Reduction of group velocities lowers the lattice thermal conductivity to the green dashed line. Lifetime reductions due to strong boundary scattering associated with disorder reduces the conductivity to the green band. Adding the effect of both group velocity reduction as well as lowered lifetime as a result of increased scattering reduces the predicted lattice thermal conductivity to the yellow band.

in Fig. 4.1). If the effect of group velocity and lifetime reduction are combined one obtains a lattice thermal conductivity that is comparable to the measured data (yellow band in Fig. 4.1).

The results show that a reduction of $\kappa_\perp$ by 40–60% can be achieved merely by variations in the layer stacking, which is associated with only a small energy cost. This can be important for e.g., thermoelectric applications where a low thermal conductivity in conjunction with a high electrical conductivity is necessary to achieve a high thermodynamic efficiency. Since electrons typically have larger mean free paths than phonons, they are less likely to be affected by changes in the stacking order, thus creating the possibility to decouple electrical and thermal transport properties. While the model was developed for WSe_2 it is likely to be also applicable to similar vdW solids.

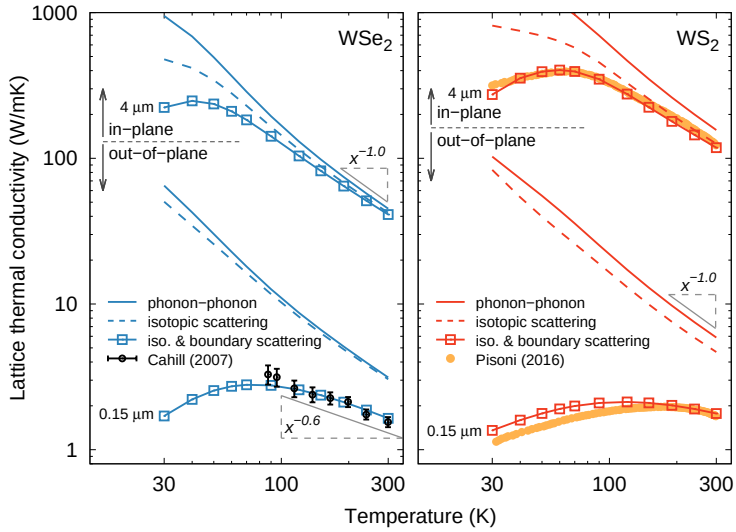

Figure 4.2: Calculated lattice thermal conductivity of WSe_2 and WS_2 in comparison with experiment. Solid and dashed lines and lines with squares shoe the calculated thermal conductivity obtained when including boundary scattering, isotopic scattering and boundary scattering. The structural length scale is set to 4 μm for the in-plane and 0.15 μm for the out-of-plane conductivity. Experimental data for WS_2 and WSe_2 were taken from Pisoni (2016) [45] and Chiritescu (2007) [44], respectively.

4.2 Paper II: Thermal conductivity in van der Waals solids

Novel synthesis techniques [29, 101] provide the opportunity to create highly engineered van der Waals (vdW) solids, which emerge as promising candidates for a manifold of applications including electronic components [36], optoelectronic [34, 37, 38], thermoelectrics [40], and spintronics [39]. Since thermal transport plays a key role in many of these situations, it is important to develop a detailed understanding of the thermal conductivity κ in vdW solids.

Unfortunately, values for the thermal conductivities reported in the literature exhibit a wide spread and can differ by more than one order of magnitude. This can be partly attributed to the challenges associated with experimental measurements of the thermal conductivity in nanostructures with pronounced anisotropy, see e.g., [49]. Possibly even more crucial is the sensitivity of the results to defects and sample size effects, as the growth of large high-quality TMD single crystals is very time consuming [49].

Given this motivation the present paper investigates the finite temperature prop-

erties as well as the lattice thermal conductivity κ in Mo and W-based transition metal dichalcogenides (TMDs) employing a combination of density functional and Boltzmann transport theory. Once again the calculations were carried out using the vdW-DF-CX functional, which is shown to yield excellent agreement with experimental lattice constants at room temperature with an average relative error below 0.2%.

With regard to the thermal conductivity it is demonstrated that care must be taken with regard to some computational parameters, in particular the displacement amplitude used for evaluating finite differences. A careful analysis shows that larger values than commonly used for e.g., materials such as silicon, are required in order to balance numerical accuracy with the smallness of vdW forces.

The calculated in-plane conductivities at room temperature are in good agreement with experimental data for high-purity material, when only phonon-phonon and isotopic scattering are included (Fig. 4.2). Explaining the experimental data over the entire temperature, however, requires inclusion of a temperature independent scattering mechanism that limits the phonon mean free path (MFP). The latter effect is even more pronounced in the case of the out-of-plane conductivity (Fig. 4.2).

The sensitivity of the thermal conductivity to structural inhomogeneities can be rationalized in terms of the long MFPs of the modes that contribute the most strongly to κ. The MFP of these modes (including phonon-phonon and isotopic scattering) is at least 1 μm, which is comparable to silicon but much larger than e.g., PbTe. This behavior is promising for thermoelectric applications, where lowering the lattice part of the thermal conductivity is a widely employed approach for increasing the thermodynamic efficiency. On the other hand, it can pose problems for electronic and optoelectronic applications, which require a large κ for rapid heat dissipation.

Overall the present study provides a comprehensive set of lattice thermal conductivities for bulk TMDs that establishes bounds set by phonon-phonon scattering and intrinsic length scales. It thereby forms the basis for future studies on these systems, which could focus e.g., on genuine vdW solids comprising different layers.

4.3 Paper III: Chemical order and transport properties in an inorganic clathrate: Optimal structures by computational design

Clathrates are chemical substances with a defined lattice structure that can trap atomic or molecular species [50, 51]. Inorganic clathrates such as $Ba_8Ga_{16}Ge_{30}$ or $Sr_8Ga_{16}Sn_{30}$ exhibit a combination of electrical and thermal transport properties

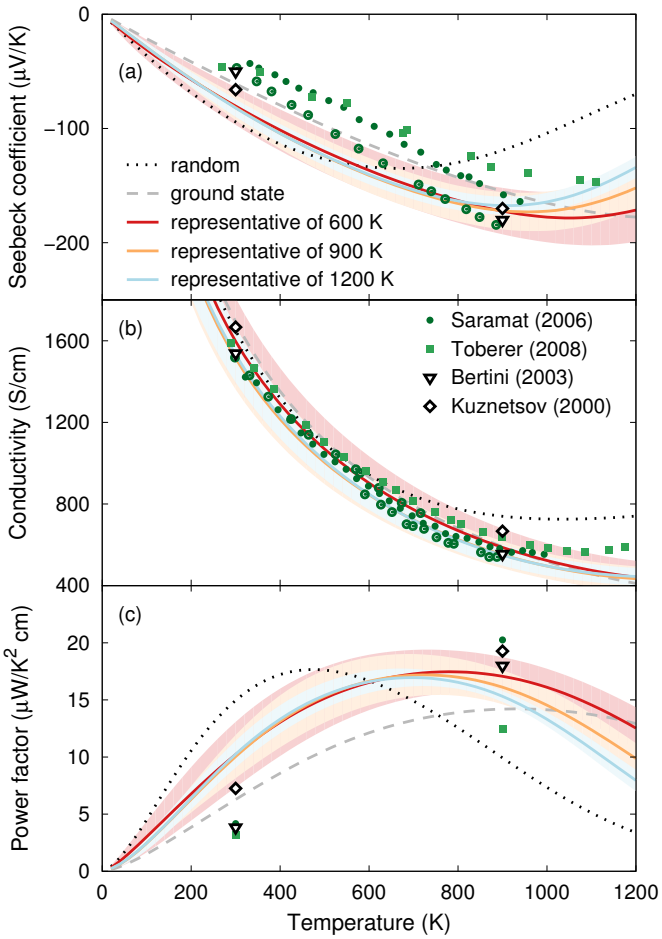

Figure 4.3: Electrical transport properties of *n*-type $Ba_8Ga_{16}Ge_{30}$ at a carrier density of 3×10^{20} cm^{-3}. (a) Seebeck coefficient, (b) electrical conductivity, and (c) power factor as a function of temperature from calculations in comparison with experimental data.

that are very favorable for thermoelectric applications [52, 53]. Here, the earth alkaline atoms act as guest species that occupy the cages provided by the host structure, where the host structure most commonly is composed of elements from groups 13 and 14. Clathrates, as well as some other thermoelectric materials, are multicomponent systems exhibiting chemical ordering, with the potential to affect transport properties.

This paper focuses on the electrical properties of $Ba_8Ga_{16}Ge_{30}$ due to the chemical order, investigated with the use of alloy cluster expansions. The cluster expansions were trained by density functional theory calculations, in which the chemical order in the form of the site occupancy factors was determined as a function of

temperature. A ground-state structure was determined with the use of a simulated annealing procedure. The ground-state was shown not to have any first neighbor Ga–Ga bonds.

The electrical conductivity σ and Seebeck coefficient S could then be computed under n-type conditions for the ground-state structure, as well as for representative configurations for the chemical order at different temperatures (Fig. 4.3). These computations were conducted using a combination of density functional theory and Boltzmann transport theory, showing good agreement with experimental data for both the electrical conductivity and the power factor $S^2\sigma$. The power factor was shown to peak roughly at 800-900 K consistent with previous experiments.

Finally, by combining density functional theory, Boltzmann transport theory, and Monte Carlo simulations with cluster expansions, a maximization of the power factor could be achieved by searching for optimized configurations. It was found that minimizing the Ga SOFs at the 6*c* Wyckoff site gives a calculated power factor up to 27 μW/K^{2}cm. The optimized power factors corresponds to an increase of approximately 60% compared to the power factor of non-optimized configurations.

4.4 Paper IV: Electronic and lattice thermal conductivity in intermetallic clathrates: A first principles perspective

Inorganic clathrates are among the most efficient thermoelectric materials [67, 102] with reported figure-of-merit (zT) exceeding values of one [56, 58]. They generally exhibit very low thermal conductivities, comparable to the conductivities of glasses. Hence, inorganic clathrates are though of as realizations of the "phonon glass-electron crystal" concept [13]. The low thermal conductivity originates partly from the heavier caged guest species, which undergo "rattling" motion at low frequencies, due to weak binding. In this paper both the electronic and the lattice thermal conductivity in the representative inorganic clathrate $Ba_8Ga_{16}Ge_{30}$ were investigated in detail. The ground-state configuration, as well as some other representative configurations obtained in Paper III, were used for this purpose.

The lattice thermal conductivity in $Ba_8Ga_{16}Ge_{30}$ is challenging to compute, in part due to the sensitivity to the vibrational spectra of the guest rattlers. The phonon dispersion was calculated from the second order interatomic force constants (IFCs) obtained with density functional theory. The IFCs were then used to examine the thermal expansion within the quasi-harmonic approximation. Because of the impact of the structure on the rattler-modes, the choice of exchange-correlation functional was first scrutinized. The non-empirical consistent-exchange van der Waals functional (vdW-DF-cx) [96] was found to be well suited, compared

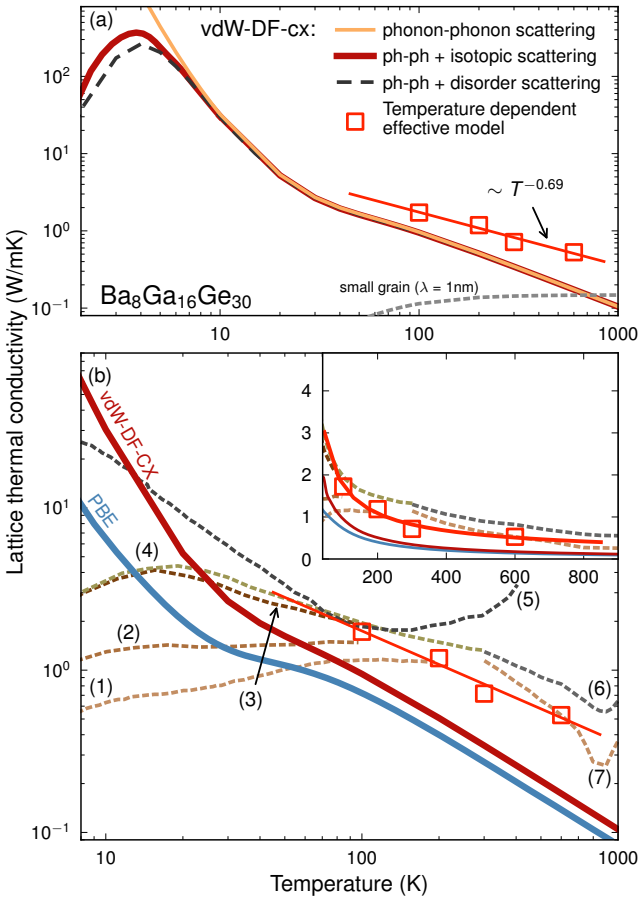

Figure 4.4: Lattice thermal conductivity κ_l of $Ba_8Ga_{16}Ge_{30}$ as a function of temperature. (a) Comparison of κ_l due to different included scattering channels, calculated using IFCs achieved with the vdW-DF-cx functional, as well as a comparison to the computations using temperature dependent effective IFCs. (b) Comparison between computations, using IFCs from the vdW-DF-cx functional (red solid line), the PBE functional (solid blue line), temperature dependent effective models (squares) and experimental data sets (dashed lines marked by numbers). The inset shows the same data on a linear scale. Different experimental data sets are marked (1)-(7).

to the PBE functional, since it predicted a finite temperature lattice constant closer to the experimental data and produced a better vibrational spectrum when compared to the data in Ref. [68].

To address the lattice thermal conductivity the third order IFCs were computed. The static (0 K) IFCs produced lattice thermal conductivities that were systemat-

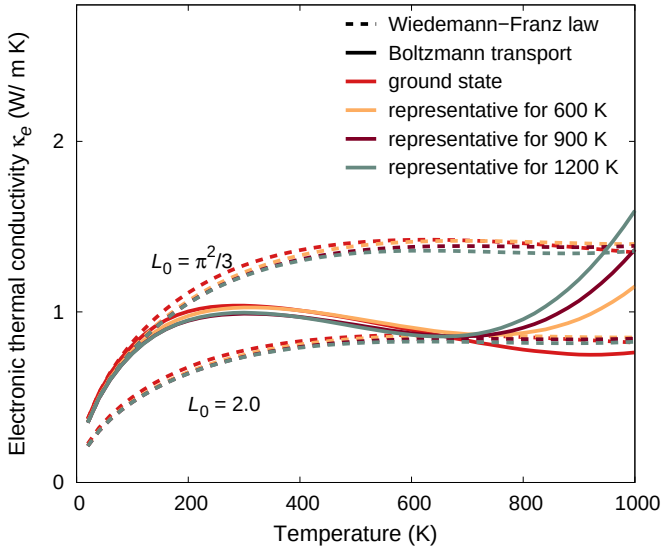

Figure 4.5: Electronic contribution κ_e to the thermal conductivity calculated for the ground state structure as well as for structures extracted from Monte Carlo simulations representative of the chemical order at different temperatures. Data obtained using the Wiedemann-Franz law $\kappa_e = L\sigma T$ are shown by dashed lines, whereas the thermal conductivity obtained within the framework of Boltzmann transport theory is shown by solid lines.

ically underestimating the reported experimental conductivities (Fig. 4.4). Using effective temperature dependent IFCs, obtained with first-principles molecular dynamics simulations, the prediction improved both in magnitude and slope. The success of the effective IFCs indicates that phonon-phonon coupling is important for an accurate representation of the low-frequency region related to the rattler-modes. In agreement with previous work the low-lying guest modes were associated with an avoided band crossing in the phonon dispersion [63, 68]. The underestimation of the rattler modes was linked with the onset of the avoided band crossing at a lower $\boldsymbol{q}$ vector. In addition to the previous studies, which focused on the low energy region, modes at higher energies were identified to contribute to the lattice thermal conductivity significantly.

The electronic contribution to the thermal conductivity was investigated using Boltzmann transport theory, by applying it to the ground-state and some higher temperature configurations. According to Wiedemann-Franz law couples the electronic part of the thermal conductivity κ_e to the electrical conductivity σ through the relation

$$\kappa_e = L\sigma T, \tag{4.1}$$

where $L = L_0(k_B^2/e^2)$ is the Lorenz number. The Wiedemann-Franz law is used to separate the electronic thermal conductivity and the lattice thermal conductivity from the measured total thermal conductivity. The value of L_0 typical ranges from 2 (for semiconductors) to 3.3 (for a degenerate electron gas). The computed κ_e lies between conductivities predicted by Wiedemann-Franz law using these L_0 values (Fig. 4.5). It was seen that lower temperatures are more consistent with the larger Lorenz-factor, and conductivities at higher temperatures are more consistent with the Lorenz-factor typical for a semiconductor. This variation indicates that special care should be taken when applying the Wiedemann-Franz law for interpreting measured thermal conductivities of clathrate systems, especially since the electronic thermal conductivity is of the same order as the lattice thermal conductivity.

5

Outlook

In the present thesis, two different types of materials were investigated with regard to their ability to transport heat. Papers I and II addressed layered materials with very anisotropic properties. Because of the weak interlayer binding, they are prone to form planar defects, which as shown in this thesis can have dramatic effects on their ability to conduct heat. At the same time, the 2D character of the individual sheets enables the fabrication of heterostructures composed of layers of different 2D materials including but not limited to the transition metal dichalcogenides (TMDs) investigated in the present thesis. Thus while in the present thesis the focus has been on homogeneous materials, in the future this research ought to be extended to heterostructures composed of different TMDs and not necessarily limited to Mo and W-based compounds. It was discussed in Paper II how differences in mass and structure affect the phonon dispersion, which in turn determines to a large extent the lattice thermal conductivity. By combining different layers, it becomes possible to engineer these features and to manipulate both out-of-plane and in-plane transport in a very controlled fashion.

The approach taken in Paper III is here potentially very powerful, i.e., by combining transport calculations with effective models (such as the cluster expansions in Paper III) and sampling techniques (e.g., Monte Carlo simulations or genetic algorithms) one can computationally design structures with specified transport properties. This "inverse design" approach was adopted in Paper III to optimize electrical transport properties in clathrates but is in principle equally applicable to thermal transport. Conversely, it would be interesting to explore electrical transport in van der Waals solids and specifically to explore strategies for controlling electron-phonon coupling and decoupling electronic and thermal transport.

Besides planar defects are different point defects in the TMDs interesting to investigate. As a result of the manufacturing process for single or few-layers TMDs,

in conjunction with low defect formation energies for point defects, can considerable defect concentrations be expected, and with that the possibility for substantial effects on the thermal conductivity [103]. For this investigation is a first-principles Greens-function approach [104] suitable for quantifying the effect of scattering due to point defects.

The use of effective interatomic force constants in Paper IV was crucial for a functional description of the rattler-modes and with that the correct prediction of the lattice thermal conductivity. This approach could be interesting to apply for other systems, e.g., filled skutterudites, that also show signs of strongly damped quasi-particles when described with static interatomic force constants [105]. A more rigorous approach is also desirable. The effective model takes the phonon-phonon coupling with the vibrational spectra into account. Applying self-consistent phonon theory, for renormalization of the spectra, would be an interesting step.

The insight and results gained in this thesis are not only important for our understanding of van der Waals solids and thermoelectric materials but for thermal transport in general. In the future, the goal will be to implement the concepts developed here in experimental settings and to push the limits of materials and transport. In this fashion this thesis will ultimately contribute to the vast and important field of energy management.

A

Balance equations in thermodynamics

The fundamental questions within theories dealing with transport, are how much of a quantity is within a specific region of space, and in which way is this amount changing over time? In general there are only three different kinds of mechanisms that can change the amount of quantity within the region. The quantity can be transported over the boundary to the surroundings, or the quantity can be either produced or annihilated within the boundary. The mathematical relations describing theses processes are called *balance equations*.

Under the assumption that the continuum hypothesis is valid, an extensive quantity E can be associated with a material point, such that

$$\lim_{\Delta M \to 0} \frac{\Delta E}{\Delta V} = \rho e, \tag{A.1}$$

where M is the mass occupying the volume V, ρ is the mass density and e the specific value of E. Given a description of the specific distribution of a quantity, the total quantity within a region Ω is then given by summing up all contributions

$$E_\Omega = \int_\Omega \rho e \, \mathrm{d}V, \tag{A.2}$$

where $\mathrm{d}V$ is the volume element to Ω. With the use of the Reynolds transport theorem [106], the rate of change of E_Ω is expressed as

$$\frac{\mathrm{d}E_\Omega}{\mathrm{d}t} = \frac{\mathrm{d}}{\mathrm{d}t} \int_\Omega \rho e \, \mathrm{d}V = \int_\Omega \rho \frac{\partial e}{\partial t} \, \mathrm{d}V, \tag{A.3}$$

where the partial derivative is in the local sense. In principle, as stated in the introduction to this section, the only possibility to change the ammount of the quantity within Ω is to either have the quantity leave or enter the boundary $\partial\Omega$, or that the quantity is produced or annihilated within Ω. The flow of the quantity e is readily described as a flux $\boldsymbol{J}_e$. Each component of the flux, by definition, is the amount of E flowing through a unit area perpendicular to the corresponding unit vector, in unit time. Defining $\boldsymbol{n}$ as the outbound normal to $\partial\Omega$, the total flow F entering Ω through the boundary in unit time is then

$$F = -\int_{\partial\Omega} \boldsymbol{J}_e \cdot \boldsymbol{n}\, \mathrm{d}S = -\int_{\Omega} \nabla \cdot \boldsymbol{J}_e\, \mathrm{d}V. \tag{A.4}$$

Here, $\mathrm{d}S$ is the surface element to $\partial\Omega$ and the divergence theorem is used to transform the expression into a volume integral. The rate of production is expressed by a function σ_e, that describes the local production when positive, and local annihilation when negative. The total production P in unit time within Ω, due to σ_e is then

$$P = \int_{\Omega} \sigma_e\, \mathrm{d}V. \tag{A.5}$$

By invoking the principle of balance, the rate of change within Ω is the sum of transport over the boundary and internal production

$$\frac{\mathrm{d}E_\Omega}{\mathrm{d}t} = F + P, \tag{A.6}$$

or in integral form expressed as

$$\int_{\Omega} \rho \frac{\partial e}{\partial t}\, \mathrm{d}V = -\int_{\Omega} \nabla \cdot \boldsymbol{J}_e\, \mathrm{d}V + \int_{\Omega} \sigma_e\, \mathrm{d}V. \tag{A.7}$$

The integrals are over the same volume, and since the volume element is arbitrary the integrand must vanish identically. The general balance law, written in local form, is then

$$\rho \frac{\partial e}{\partial t} = -\nabla \cdot \boldsymbol{J}_e + \sigma_e. \tag{A.8}$$

In the special case where the quantity is only exchanged through fluxes, i.e., when there is no production term, the quantity is said to be conserved and the balance equation may be expressed as

$$\rho \frac{\partial e}{\partial t} + \nabla \cdot \boldsymbol{J}_e = 0, \tag{A.9}$$

which takes on the simple form of a *conserved continuity equation*.

A.1 Balance equations for the internal energy

From the broader perspective, *the first law of thermodynamics* implicitly invokes a balance law, simply stating that the *total energy* is conserved. For practical purposes, some context is needed. Within the context of continuum mechanics, the law states that the material derivative of the total energy of a body equals the total power input from both work W and heat Q

$$\frac{\mathrm{d}K}{\mathrm{d}t} + \frac{\mathrm{d}U}{\mathrm{d}t} = W + Q. \tag{A.10}$$

Where K is the macroscopic kinetic energy and U the internal energy. The input from work associates with two types of processes affecting the macroscopic state of the system, either acceleration and deformation of the bulk due to coupling to external fields or deformation and acceleration of the boundaries due to external traction. Heat can be either in the form of a heat flux $\boldsymbol{J}_q$ over the system boundary, or from internal generation σ_q. Internal generation can originate, e.g., from radioactive decay, or in the case of fluids from frictional losses due to viscous interaction with the surroundings as well as turbulent internal dissipation, or in the case of an electric current transmitted through the system from irreversible energy transfer due to Joule heating.

Following a standard treatment, such as the one in Reddy [107], the first law, Eq. (A.10), gives the local form of energy balance for the internal energy density u, expressed as

$$\rho\frac{\mathrm{d}u}{\mathrm{d}t} = -\nabla\cdot\boldsymbol{J}_q + \sigma : S + \sigma_q. \tag{A.11}$$

Here $\sigma : S$ is the double scalar product[1] between the internal stress tensor and the symmetric part of the strain rate tensor. The term has the interpretation of a source due to internal work.

In the case of a transmitted electric current, the electrons is accelerated in a collective manner due to a difference in the electric potential, introducing a drift velocity to the electron population. At the same time the electrons scatter, which introduces a random component in the velocity distribution. The result is an increase in the part of the entropy pertaining to the electrons, introducing a dissipation of the kinetic energy carried in the field direction.

$$\rho\frac{\mathrm{d}u}{\mathrm{d}t} = -\nabla\cdot\boldsymbol{J}_q + \sigma : S + \boldsymbol{E}\cdot\boldsymbol{i}. \tag{A.12}$$

[1]The double scalar product is here defined as the double sum $A : B = \sum ij A_{ij} B_{ji}$.

A.2 Balance equations for entropy

In classical thermodynamics, the entropy S_0 is only defined for systems in equilibrium. In non-equilibrium thermodynamics, due to the local-equilibrium hypothesis the entropy concept can be extended to systems out of equilibrium, resulting in an extensive quantity S that must obey a transport law of its own.

Since entropy is an extensive quantity, it is reasonable to separate changes in a systems entropy into an entropy flow $\boldsymbol{J}_s$, and an entropy production σ_s. As stated with *the second law of thermodynamics*, entropy is a *non-conserved quantity* that can not be annihilated. Hence the production term must be either zero or greater than zero

$$\sigma_s \geq 0. \tag{A.13}$$

This is a stronger statement than the one given in classical thermodynamics, where the increase of entropy is assumed to be increasing globally.

The balance equation for the change of a systems entropy is now expressed as

$$\frac{\mathrm{d}S}{\mathrm{d}t} = \frac{\mathrm{d}_e S}{\mathrm{d}t} + \frac{\mathrm{d}_i S}{\mathrm{d}t}. \tag{A.14}$$

Here the total entropy is given by integrating the specific entropy s

$$S = \int_\Omega \rho s \, \mathrm{d}V. \tag{A.15}$$

The exchange of entropy with the surroundings is expressed through the entropy flux

$$\frac{\mathrm{d}_e S}{\mathrm{d}t} \int_{\partial\Omega} \boldsymbol{J}_s \, \mathrm{d}S, \tag{A.16}$$

and the internal production is

$$\frac{\mathrm{d}_i S}{\mathrm{d}t} \int_\Omega \sigma_s \, \mathrm{d}V. \tag{A.17}$$

By invoking the divergence and the Reynold's transport theorems the equation for local entropy balance is

$$\rho \frac{\mathrm{d}s}{\mathrm{d}t} = -\nabla \cdot \boldsymbol{J}_s + \sigma_s. \tag{A.18}$$

B

Liouville's theorem

The following short section gives a derivation of *Liouville's theorem*. This theorem is of importances in the theoretical framework of a statistical treatment of transport phenomena [108] and the foundation on which the *Boltzmann equation* is formally derived.

Start by introducing a compact notation for the $6N$ generalized coordinates and momenta in phase space as $q = q_1, \dots, q_{3N}$ and $p = p_1, \dots, p_{3N}$. Let the corresponding volume element be $dqdp = dq_1 \cdots dq_{3N} dp_1 \cdots dp_{3N}$. Let $\rho(q, p, t)$ be the number density of states in phases space so that

$$\rho(q, p, t)\, dqdp \tag{B.1}$$

corresponds to the number of states in the volume element at time t. Let V be a constant volume in phase space and S the surface that enclose V. The rate of change in the number of states in V is then

$$\frac{\partial}{\partial t} \int_V \rho\, dqdp. \tag{B.2}$$

As long as no states are produced or destroyed within V the rate at wich the number of states changes must equal the net transport of states over S

$$\frac{\partial}{\partial t} \int_V \rho\ dqdp = -\int_S \rho\, \boldsymbol{v} \cdot \boldsymbol{n}\, dS. \tag{B.3}$$

Here $\boldsymbol{v}$ is the velocity field [1] across the surface and $\boldsymbol{n}$ the outbound normal. Using

[1] A velocity field in the generalized sense that

$$\boldsymbol{v} = \Big(\frac{\partial q_1}{\partial t}, \dots, \frac{\partial q_{3N}}{\partial t}, \frac{\partial q_1}{\partial t}, \dots, \frac{\partial p_{3N}}{\partial t} \Big).$$

the divergence theorem the surface integral can be changed into a volume integral over the divergence of $\rho\boldsymbol{v}$. Since the control volume is not changing the time derivative can be taken inside the volume integral over ρ and a re-arrangement gives

$$\int_V \Big(\frac{\partial \rho}{\partial t} + \nabla \cdot (\rho \boldsymbol{v})\Big) dV = 0. \tag{B.4}$$

The volume is arbitrarily chosen so the integrand must vanish identically. Hence

$$\frac{\partial \rho}{\partial t} + \nabla \cdot (\rho \boldsymbol{v}) = 0. \tag{B.5}$$

Applying the product rule on the terms in the expanded divergence in the continuity equation equals

$$\frac{\partial \rho}{\partial t} + \sum_{i=1}^{3N} \Big(\frac{\partial \rho}{\partial q_i}\frac{\partial q_i}{\partial t} + \frac{\partial \rho}{\partial p_i}\frac{\partial p_i}{\partial t} \Big) + \rho \sum_{i}^{3N} \Big(\frac{\partial^2 q_i}{\partial q_i \partial t} + \frac{\partial^2 p_i}{\partial p_i \partial t} \Big) = 0. \tag{B.6}$$

For each pair of conjugate variables the canonical equations read [109]

$$\begin{aligned} \frac{\partial q_i}{\partial t} &= \quad \frac{\partial H}{\partial p_i} \\ \frac{\partial p_i}{\partial t} &= -\frac{\partial H}{\partial q_i}, \end{aligned} \tag{B.7}$$

where $H(q, p)$ is the Hamiltonian, and so each term in the last sum in Eq. (B.6) is identically zero since partial derivatives commute. Due to the chain rule combined with the Poisson bracket [2] the remaining part of the continuity equation can now be written as the total derivative

$$\begin{aligned} \frac{d\rho}{dt} &= \frac{\partial \rho}{\partial t} + \sum_{i=1}^{3N} \Big(\frac{\partial \rho}{\partial q_i}\frac{\partial q_i}{\partial t} + \frac{\partial \rho}{\partial p_i}\frac{\partial p_i}{\partial t} \Big) \\ &= \frac{\partial \rho}{\partial t} + \sum_{i=1}^{3N} \Big(\frac{\partial \rho}{\partial q_i}\frac{\partial H}{\partial p_i} - \frac{\partial \rho}{\partial p_i}\frac{\partial H}{\partial q_i} \Big) \\ &= \frac{\partial \rho}{\partial t} + \big\{\rho, H\big\} = 0. \end{aligned} \tag{B.8}$$

[2] The Poisson bracket for a quantity A related to a dynamical system governed by the Hamiltonian H is defined as

$$\big\{A, H\big\} = \sum_{i=1}^{3N} \Big(\frac{\partial A}{\partial q_i}\frac{\partial H}{\partial p_i} - \frac{\partial A}{\partial p_i}\frac{\partial H}{\partial q_i} \Big).$$

This resembles the result for an incompressibel fluid and one can think of the number densities of states in phase space as constituting an incompressible fluid. In the fixed frame of reference it is then shown that the total derivative of the number density function is zero. In the opposite frame, the co-moving frame that follows the fluid motion the number density doesn't change with time. This has the implication that a volume element in phase-space is invariant over time. This is the result known as *Liouville's theorem* and equation Eq. (B.8) is called *Liouville's equation*.

Acknowledgments

I would first of all like to express my sincerest gratitude to my supervisor Paul Erhart, who gave me the opportunity to do this work. His knowledge, dedication, and not the least patience, has made this thesis possible.

Secondly, I would like to express gratitude to my examiner Göran Wahnström. His kindness, and not the least patience, has been much appreciated. It was also he who initially helped invoke my interest for computational work and coding, many years ago when I attended his course in computational physics.

Thirdly, my office mates. Both my prior, Leili Gharaee, and recent one in Tuomas Rossi. You have both been wonderful to share office with, always up and ready for interesting, and usually very helpful, discussions.

Blender skills are not to be forgotten, many thanks to Mattias Ångqvist for the cover picture. (And for being awesome in general. Even if you are not tall enough for writing multi-threaded code, but who is…?).

And for the rest of the group, you are all a crucial part in creating the best of working places.

Adam, consider yourself acknowledged, one more time. It has been so much fun teaching together with you.

I would also like to take the opportunity to thank Prof. Georg Madsen at TU Wien, the opportunity to visit your group in Vienna was much appreciated. And many warm thanks to Jesús Carrete Montaña, whose kindness and hospitality made my stay in Vienna extra delightful.

And finally, this thesis is dedicated to my family. My brothers, Joakim and Joel, with their families. My parents Hans and Kerstin. And most of all my wonderful wife Hanna, and my daughters Nova and Lilo. I love you all so much.

Bibliography

[1] M. Kardar, *Statistical Physics of Particles*, 1 edition ed. (Cambridge University Press, Cambridge : New York, 2007).

[2] International Energy Agency, *Key World Energy Statistics 2015*, http://www.iea.org, 2015, accessed: 2016-05-14.

[3] R. Bookstaber, *A Demon of Our Own Design: Markets, Hedge Funds, and the Perils of Financial Innovation* (Wiley, Hoboken, N. J., 2008).

[4] United Nations - Department of Economic and Social Affairs, http://esa.un.org/unpd/wpp/Download/Standard/Population/, data accessed: 2016-05-14.

[5] H. D. Klemme and G. F. Ulmishek, *Effective Petroleum Source Rocks of the World: Stratigraphic Distribution and Controlling Depositional Factors (1)*, AAPG Bulletin **75**, 1809 (1991).

[6] G. Bowden, *The Social Construction of Validity in Estimates of US Crude Oil Reserves*, Social Studies of Science **15**, 207 (1985).

[7] K. Aleklett, M. Lardelli, and O. Qvennerstedt, *Peeking at peak oil* (Springer, New York ; London, 2012).

[8] K. Aleklett, M. Höök, K. Jakobsson, M. Lardelli, S. Snowden, and B. Söderbergh, *The Peak of the Oil Age – Analyzing the world oil production Reference Scenario in World Energy Outlook 2008*, Energy Policy **38**, 1398 (2008).

[9] I. Chapman, *The end of Peak Oil? Why this topic is still relevant despite recent denials*, Energy Policy **64**, 93 (2014).

[10] U. S. Energy Information Agency, *International Energy Statistics - Total Primary Energy Production*, http://www.eia.gov/cfapps/ipdbproject/IEDIndex3.cfm, data accessed: 2016-05-14.

[11] Intergovernmental Panel on Climate Change, *Climate Change 2013 - The Physical Science Basis: Working Group I Contribution to the Fifth Assessment Report of the Intergovernmental Panel on Climate Change*, 1 edition ed. (Cambridge University Press, New York, 2014).

[12] Y. Demirel, *Energy: production, conversion, storage, conservation, and coupling*, *Green energy and technology* (Springer, London ; New York, 2012).

[13] *CRC Handbook of Thermoelectrics*, 1 edition ed., edited by D. M. Rowe (CRC Press, Boca Raton, FL, 1995).

[14] D. M. Rowe, *Thermoelectrics handbook: macro to nano-structured materials* (CRC Press, Boca Raton, FL, 2005).

[15] H. B. Callen, *Thermodynamics and an introduction to thermostatistics* (Wiley, New York, 1985).

[16] S. R. D. Groot and P. Mazur, *Non-Equilibrium Thermodynamics*, dover ed edition ed. (Dover Publications, New York, 2011).

[17] *Thermoelectrics Handbook: Macro to Nano*, edited by D. Rowe (CRC Press, Boca Raton, 2005).

[18] J. M. Ziman, *Electrons and phonons* (Clarendon Press, Oxford, 1960).

[19] H. Goldstein, *Classical Mechanics*, 2nd edition ed. (Addison-Wesley, Reading, Mass, 1980).

[20] J. J. Sakurai and S. F. Tuan, *Modern quantum mechanics*, rev. ed ed. (Addison-Wesley, Reading, Mass, 1994).

[21] G. P. Srivastava, *The physics of phonons* (Hilger, Bristol, 1990).

[22] W. Li, J. Carrete, N. A. Katcho, and N. Mingo, *ShengBTE: A solver of the Boltzmann transport equation for phonons*, Comp. Phys. Comm. **185**, 1747 (2014).

[23] A. Togo, L. Chaput, and I. Tanaka, *Distributions of phonon lifetimes in Brillouin zones*, Phys. Rev. B **91**, 094306 (2015).

[24] A. Gupta, T. Sakthivel, and S. Seal, *Recent development in 2D materials beyond graphene*, Progress in Materials Science **73**, 44 (2015).

[25] K. S. Novoselov, A. Mishchenko, A. Carvalho, and A. H. Castro Neto, *2D materials and van der Waals heterostructures.*, Science (New York, N.Y.) **353**, aac9439 (2016).

[26] R. Mas-Ballesté, C. Gómez-Navarro, J. Gómez-Herrero, and F. Zamora, *2D materials: to graphene and beyond*, Nanoscale **3**, 20 (2011).

[27] K. S. Novoselov, A. K. Geim, S. V. Morozov, D. Jiang, Y. Zhang, S. V. Dubonos, I. V. Grigorieva, and A. A. Firsov, *Electric Field Effect in Atomically Thin Carbon Films*, Science **306**, 666 (2004).

[28] H. Liu, A. T. Neal, Z. Zhu, Z. Luo, X. Xu, D. Tománek, and P. D. Ye, *Phosphorene: An Unexplored 2D Semiconductor with a High Hole Mobility*, ACS Nano **8**, 4033 (2014).

[29] A. K. Geim and I. V. Grigorieva, *Van der Waals heterostructures*, Nature **499**, 419 (2013).

[30] K. Watanabe, T. Taniguchi, and H. Kanda, *Direct-bandgap properties and evidence for ultraviolet lasing of hexagonal boron nitride single crystal*, Nature Materials **3**, 404 (2004).

[31] P. J. Zomer, S. P. Dash, N. Tombros, and B. J. Van Wees, *A transfer technique for high mobility graphene devices on commercially available hexagonal boron nitride*, Applied Physics Letters **99**, 2009 (2011).

[32] C. R. Dean, A. F. Young, I. Meric, C. Lee, L. Wang, S. Sorgenfrei, K. Watanabe, T. Taniguchi, P. Kim, K. L. Shepard, and J. Hone, *Boron nitride substrates for high-quality graphene electronics*, Nature Nanotechnology **5**, 722 (2010).

[33] W. Rindler, *Introduction to special relativity* (Clarendon Press, Oxford, 1991).

[34] Q. H. Wang, K. Kalantar-Zadeh, A. Kis, J. N. Coleman, and M. S. Strano, *Electronics and optoelectronics of two-dimensional transition metal dichalcogenides*, Nature Nanotech. **7**, 699 (2012).

[35] G. Gao, W. Gao, E. Cannuccia, J. Taha-Tijerina, L. Balicas, A. Mathkar, T. N. Narayanan, Z. Liu, B. K. Gupta, J. Peng, Y. Yin, A. Rubio, and P. M. Ajayan, *Artificially Stacked Atomic Layers: Toward New van der Waals Solids*, Nano Lett. **12**, 3518 (2012).

[36] B. Radisavljevic, A. Radenovic, J. Brivio, V. Giacometti, and A. Kis, *Single-layer MoS_2 transistors*, Nature Nanotech. **6**, 147 (2011).

[37] X. Hong, J. Kim, S.-F. Shi, Y. Zhang, C. Jin, Y. Sun, S. Tongay, J. Wu, Y. Zhang, and F. Wang, *Ultrafast charge transfer in atomically thin MoS_2/WS_2 heterostructures*, Nature Nanotech. **9**, 682 (2014).

[38] M. Massicotte, P. Schmidt, F. Vialla, K. G. Schädler, A. Reserbat-Plantey, K. Watanabe, T. Taniguchi, K. J. Tielrooij, and F. H. L. Koppens, *Picosecond photoresponse in van der Waals heterostructures*, Nature Nanotech. **11**, 42 (2016).

[39] W. Han, *Perspectives for spintronics in 2D materials*, APL Materials **4**, 032401 (2016).

[40] H. Guo, T. Yang, P. Tao, Y. Wang, and Z. Zhang, *High pressure effect on structure, electronic structure, and thermoelectric properties of MoS_2*, J. Appl. Phys. **113**, 013709 (2013).

[41] S. Thakurta and A. Dutta, *Electrical conductivity, thermoelectric power and hall effect in p-type molybdenite (MoS2) crystal*, Journal of Physics and Chemistry of Solids **44**, 407 (1983).

[42] J.-Y. Kim, S.-M. Choi, W.-S. Seo, and W.-S. Cho, *Thermal and Electronic Properties of Exfoliated Metal Chalcogenides*, Bulletin of the Korean Chemical Society **31**, 3225 (2010).

[43] A. L. Moore and L. Shi, *Emerging challenges and materials for thermal management of electronics*, Materials Today **17**, 163 (2014).

[44] C. Chiritescu, D. G. Cahill, N. Nguyen, D. Johnson, A. Bodapati, P. Keblinski, and P. Zschack, *Ultralow Thermal Conductivity in Disordered, Layered WSe_2 Crystals*, Science **315**, 351 (2007).

[45] A. Pisoni, J. Jacimovic, R. Gaál, B. Náfrádi, H. Berger, Z. Revay, and L. Forró, *Anisotropic transport properties of tungsten disulfide*, Scripta Materialia **114**, 48 (2016).

[46] P. Jiang, X. Qian, X. Gu, and R. Yang, *Probing Anisotropic Thermal Conductivity of Transition Metal Dichalcogenides MX2 (M = Mo, W and X = S, Se) using Time-Domain Thermoreflectance*, Advanced Materials **29**, 1 (2017).

[47] D. G. Cahill, S. K. Watson, and R. O. Pohl, *Lower limit to the thermal conductivity of disordered crystals*, Physical Review B **46**, 6131 (1992).

[48] A. Pisoni, J. Jacimovic, O. S. Barišic A. Walter, B. Náfrádi, P. Bugnon, A. Magrez, H. Berger, Z. Revay, and L. Forró, *The Role of Transport Agents in MoS_2 Single Crystals*, J. Phys. Chem. C **119**, 3918 (2015).

[49] J. Liu, G.-M. Choi, and D. G. Cahill, *Measurement of the anisotropic thermal conductivity of molybdenum disulfide by the time-resolved magneto-optic Kerr effect*, J. Appl. Phys. **116**, 233107 (2014).

[50] A. D. McNaught and A. Wilkinson, *IUPAC. Compendium of Chemical Terminology*, 2nd ed. (Blackwell Scientific Publications, Oxford, 1997), XML on-line corrected version: http://goldbook.iupac.org (2006-) created by M. Nic, J. Jirat, B. Kosata; updates compiled by A. Jenkins.

[51] G. P. Moss, P. A. S. Smith, and D. Tavernier, *Glossary of class names of organic compounds and reactivity intermediates based on structure (IUPAC Recommendations 1995)*, Pure and Applied Chemistry **67**, 1307 (2009).

[52] P. Rogl, *Thermoelectrics Handbook* (CRC Press, Boca Raton, 2005), Chap. 32, pp. 1–24.

[53] A. V. Shevelkov and K. Kovnir, in *Zintl Phases*, No. 139 in *Structure and Bonding*, edited by T. F. Fässler (Springer, Berlin, Heidelberg, 2011), pp. 97–142.

[54] B. C. Sales, B. C. Chakoumakos, R. Jin, J. R. Thompson, and D. Mandrus, *Structural, magnetic, thermal, and transport properties of $X_8Ga_{16}Ge_{30}$ (X=Eu, Sr, Ba) single crystals*, Phys. Rev. B **63**, 245113 (2001).

[55] J. D. Bryan, N. P. Blake, H. Metiu, G. D. Stucky, B. B. Iversen, R. D. Poulsen, and A. Bentien, *Nonstoichiometry and chemical purity effects in thermoelectric $Ba_8Ga_{16}Ge_{30}$ clathrate*, Journal of Applied Physics **92**, 7281 (2002).

[56] A. Saramat, G. Svensson, A. E. C. Palmqvist, C. Stiewe, E. Mueller, D. Platzek, S. G. K. Williams, D. M. Rowe, J. D. Bryan, and G. D. Stucky, *Large thermoelectric figure of merit at high temperature in Czochralski-grown clathrate $Ba_8Ga_{16}Ge_{30}$*, J. Appl. Phys. **99**, 023708 (2006).

[57] M. Christensen, N. Lock, J. Overgaard, and B. B. Iversen, *Crystal Structures of Thermoelectric n- and p-type $Ba_8Ga_{16}Ge_{30}$ Studied by Single Crystal, Multitemperature, Neutron Diffraction, Conventional X-ray Diffraction and Resonant Synchrotron X-ray Diffraction*, J. Am. Chem. Soc. **128**, 15657 (2006).

[58] E. S. Toberer, M. Christensen, B. B. Iversen, and G. J. Snyder, *High temperature thermoelectric efficiency in $Ba_8Ga_{16}Ge_{30}$*, Phys. Rev. B **77**, 075203 (2008).

[59] D. Cederkrantz, A. Saramat, G. J. Snyder, and A. E. C. Palmqvist, *Thermal stability and thermoelectric properties of p-type $Ba_8Ga_{16}Ge_{30}$ clathrates*, J. Appl. Phys. **106**, 074509 (2009).

[60] N. P. Blake, S. Latturner, J. D. Bryan, G. D. Stucky, and H. Metiu, *Band structures and thermoelectric properties of the clathrates $Ba_8Ga_{16}Ge_{30}$,*

$Sr_8Ga_{16}Ge_{30}$, $Ba_8Ga_{16}Si_{30}$, and $Ba_8In_{16}Sn_{30}$, J. Chem. Phys. **115**, 8060 (2001).

[61] N. P. Blake, D. Bryan, S. Latturner, L. Mollnitz, G. D. Stucky, and H. Metiu, *Structure and stability of the clathrates $Ba_8Ga_{16}Ge_{30}$, $Sr_8Ga_{16}Ge_{30}$, $Ba_8Ga_{16}Si_{30}$, and $Ba_8In_{16}Sn_{30}$*, J. Chem. Phys. **114**, 10063 (2001).

[62] G. K. H. Madsen, K. Schwarz, P. Blaha, and D. J. Singh, *Electronic structure and transport in type-I and type-VIII clathrates containing strontium, barium, and europium*, Phys. Rev. B **68**, 125212 (2003).

[63] G. K. H. Madsen and G. Santi, *Anharmonic lattice dynamics in type-I clathrates from first-principles calculations*, Phys. Rev. B **72**, 220301 (2005).

[64] M. Christensen, S. Johnsen, and B. B. Iversen, *Thermoelectric clathrates of type I*, Dalton Trans. **39**, 978 (2010).

[65] M. Ångqvist and P. Erhart, *Understanding Chemical Ordering in Intermetallic Clathrates from Atomic Scale Simulations*, Chemistry of Materials **29**, 7554 (2017).

[66] E. S. Toberer, A. Zevalkink, and G. J. Snyder, *Phonon engineering through crystal chemistry*, Journal of Materials Chemistry **21**, 15843 (2011).

[67] J. L. Cohn, G. S. Nolas, V. Fessatidis, T. H. Metcalf, and G. A. Slack, *Glasslike Heat Conduction in High-Mobility Crystalline Semiconductors*, Phys. Rev. Lett. **82**, 779 (1999).

[68] M. Christensen, A. B. Abrahamsen, N. B. Christensen, F. Juranyi, N. H. Andersen, K. Lefmann, J. Andreasson, C. R. H. Bahl, and B. B. Iversen, *Avoided crossing of rattler modes in thermoelectric materials*, Nature Mater. **7**, 811 (2008).

[69] J. Dong, O. F. Sankey, and C. W. Myles, *Theoretical Study of the Lattice Thermal Conductivity in Ge Framework Semiconductors*, Phys. Rev. Lett. **86**, 2361 (2001).

[70] M. Asen-Palmer, K. Bartkowski, E. Gmelin, M. Cardona, A. Zhernov, A. Inyushkin, A. Taldenkov, and V. Ozhogin, *Thermal conductivity of germanium crystals with different isotopic compositions*, Physical Review B - Condensed Matter and Materials Physics **56**, 9431 (1997).

[71] G. S. Nolas, J. L. Cohn, G. A. Slack, and S. B. Schujman, *Semiconducting Ge clathrates: Promising candidates for thermoelectric applications*, Applied Physics Letters **73**, 178 (1998).

[72] D. Frenkel and B. Smit, *Understanding Molecular Simulation* (Academic Press, London, 2001).

[73] L. Verlet, *Computer "Experiments" on Classical Fluids. I. Thermodynamical Properties of Lennard-Jones Molecules*, Physical Review **159**, 98 (1967).

[74] D. G. Cahill, P. V. Braun, G. Chen, D. R. Clarke, S. Fan, K. E. Goodson, P. Keblinski, W. P. King, G. D. Mahan, A. Majumdar, H. J. Maris, S. R. Phillpot, E. Pop, and L. Shi, *Nanoscale thermal transport. II. 2003–2012*, Applied Physics Reviews **1**, 011305 (2014).

[75] D. G. Cahill, W. K. Ford, K. E. Goodson, G. D. Mahan, A. Majumdar, H. J. Maris, R. Merlin, and S. R. Phillpot, *Nanoscale thermal transport*, jap **93**, 793 (2003).

[76] M. S. Green, *Markoff Random Processes and the Statistical Mechanics of Time-Dependent Phenomena. II. Irreversible Processes in Fluids*, The Journal of Chemical Physics **22**, 398 (1954).

[77] R. Kubo, M. Yokota, and S. Nakajima, *Statistical-Mechanical Theory of Irreversible Processes. II. Response to Thermal Disturbance*, Journal of the Physical Society of Japan **12**, 1203 (1957).

[78] M. Toda, R. Kubo, and N. Hashitsume, *Statistical physics. 2, Nonequilibrium statistical mechanics*, No. 31 in *Springer series in solid-state sciences*, 2. ed ed. (Springer, Berlin ; New York, 1991).

[79] P. K. Schelling, S. R. Phillpot, and P. Keblinski, *Comparison of atomic-level simulation methods for computing thermal conductivity*, Physical Review B **65**, 144306 (2002).

[80] S. Merabia and K. Termentzidis, *Thermal conductance at the interface between crystals using equilibrium and nonequilibrium molecular dynamics*, Phys. Rev. B **86**, 094303 (2012).

[81] E. Schrödinger, *An Undulatory Theory of the Mechanics of Atoms and Molecules*, Physical Review **28**, 1049 (1926).

[82] R. Shankar, *Principles of quantum mechanics*, 2. ed ed. (Plenum, New York, 1994).

[83] H. Kroemer, *Quantum Mechanics For Engineering: Materials Science and Applied Physics* (Pearson, Englewood Cliffs, N.J, 1994).

[84] M. Born, *Quantenmechanik der Stoßvorgänge*, Zeitschrift für Physik **38**, 803 (1926).

[85] R. M. Martin, *Electronic Structure* (Cambridge University Press, Cambridge, 2004).

[86] R. P. Feynman, *Forces in Molecules*, Physical Review **56**, 340 (1939).

[87] R. G. Parr and W. Yang, *Density-Functional Theory of Atoms and Molecules* (Oxford University Press, New York, 1989).

[88] P. Hohenberg and W. Kohn, *Inhomogeneous Electron Gas*, Phys. Rev. **136**, B864 (1964).

[89] P. J. Kohanoff, *Electronic Structure Calculations for Solids and Molecules: Theory and Computational Methods*, 1 edition ed. (Cambridge University Press, Cambridge, UK ; New York, 2006).

[90] W. Kohn and L. J. Sham, *Self-Consistent Equations Including Exchange and Correlation Effects*, Phys. Rev. **140**, A1133 (1965).

[91] J. P. Perdew, K. Burke, and M. Ernzerhof, *Generalized Gradient Approximation Made Simple*, Phys. Rev. Lett. **77**, 3865 (1996), erratum, *ibid.* **78**, 1396(E) (1997).

[92] D. C. Langreth, B. I. Lundqvist, S. D. Chakarova-Käck, V. R. Cooper, M. Dion, P. Hyldgaard, A. Kelkkanen, J. Kleis, L. Kong, S. Li, P. G. Moses, E. Murray, A. Puzder, H. Rydberg, E. Schröder, and T. Thonhauser, *A density functional for sparse matter*, J. Phys. Condens. Matter **21**, 084203 (2009).

[93] H. Rydberg, M. Dion, N. Jacobson, E. Schröder, P. Hyldgaard, S. I. Simak, D. C. Langreth, and B. I. Lundqvist, *Van der Waals Density Functional for Layered Structures*, Phys. Rev. Lett. **91**, 126402 (2003).

[94] M. Dion, H. Rydberg, E. Schröder, D. C. Langreth, and B. I. Lundqvist, *Van der Waals Density Functional for General Geometries*, Phys. Rev. Lett. **92**, 246401 (2004).

[95] K. Berland, C. Arter, V. R. Cooper, K. Lee, B. I. Lundqvist, E. Schröder, T. Thonhauser, and P. Hyldgaard, *van der Waals density functionals built upon the electron-gas tradition: Facing the challenge of competing interactions*, J. Chem. Phys. **140**, 18A539 (2014).

[96] K. Berland and P. Hyldgaard, *Exchange functional that tests the robustness of the plasmon description of the van der Waals density functional*, Phys. Rev. B **89**, 035412 (2014).

[97] F. Bloch, *Über die Quantenmechanik der Elektronen in Kristallgittern*, Zeitschrift für Physik **52**, 555 (1929).

[98] B. H. Bransden and C. J. Joachain, *Physics of atoms and molecules*, 2. ed ed. (Prentice Hall, Upper Saddle River, N.J, 2003).

[99] D. Vanderbilt, *Soft self-consistent pseudopotentials in a generalized eigenvalue formalism*, Phys. Rev. B **41**, 7892 (1990).

[100] P. E. Blöchl, *Projector augmented-wave method*, Phys. Rev. B **50**, 17953 (1994).

[101] Y. Gong, J. Lin, X. Wang, G. Shi, S. Lei, Z. Lin, X. Zou, G. Ye, R. Vajtai, B. I. Yakobson, H. Terrones, M. Terrones, B. K. Tay, J. Lou, S. T. Pantelides, Z. Liu, W. Zhou, and P. M. Ajayan, *Vertical and in-plane heterostructures from WS_2/MoS_2 monolayers*, Nature Mater. **13**, 1135 (2014).

[102] B. B. Iversen, A. E. Palmqvist, D. E. Cox, G. S. Nolas, G. D. Stucky, N. P. Blake, and H. Metiu, *Why are Clathrates Good Candidates for Thermoelectric Materials?*, J. Solid State Chem. **149**, 455 (2000).

[103] A. Katre, J. Carrete, B. Dongre, G. K. Madsen, and N. Mingo, *Exceptionally Strong Phonon Scattering by B Substitution in Cubic SiC*, Physical Review Letters **119**, 1 (2017).

[104] T. Wang, J. Carrete, A. Van Roekeghem, N. Mingo, and G. K. Madsen, *Ab initio phonon scattering by dislocations*, Physical Review B **95**, 1 (2017).

[105] W. Li and N. Mingo, *Thermal conductivity of fully filled skutterudites: Role of the filler*, Physical Review B - Condensed Matter and Materials Physics **89**, 1 (2014).

[106] F. Irgens, *Continuum mechanics* (Springer Science & Business Media, Berlin Heidelberg, 2008).

[107] J. N. Reddy, *An introduction to continuum mechanics*, 2. ed. ed. (Cambridge University Press, New York, 2013).

[108] L. E. Reichl, *A Modern Course in Statistical Physics*, 2 edition ed. (Wiley-VCH, New York, 1998).

[109] R. K. Pathria, *Statistical Mechanics*, 2nd ed. (Butterworth-Heinemann, Oxford, 1996).